Leakage Risk Assessment of

CO_2 Transportation by Pipeline at the

Illinois Basin Decatur Project, Decatur, Illinois

4th Quarter FY2011 Milestone:

Report on pipeline CO_2 leakage risk assessment

Alberto Mazzoldi and Curtis M. Oldenburg

Earth Sciences Division

Lawrence Berkeley National Laboratory, Berkeley, CA

October 19, 2011

Revised February 26, 2013

Acknowledgment: This work was carried out as part of the Midwest Geologic Sequestration Consortium Phase III Illinois Basin Decatur Project (IBDP) funded by the Assistant Secretary for Fossil Energy, Office of Sequestration, Hydrogen, and Clean Coal Fuels, National Energy Technology Laboratory. Additional support came from Lawrence Berkeley National Laboratory through the U.S. Department of Energy under Contract No. DE-AC02-05CH11231. We thank David Picard and P.G. Sriram (Clearstone Engineering Ltd., Calgary) for providing pipe outflow modeling results, and. Andrea Borgia (LBNL) for helpful internal review comments.

Table of Contents

List of Figures 4
List of Tables 8
Acronyms 9
Abstract 10
1. Introduction 12
2. Risk Assessment for CO_2 Pipeline Leakages 14
3. Special Considerations for CO_2 Leakage and Atmospheric Dispersion 17
3.1. Effects of CO_2 on Humans 17
3.2. CO_2 is a Dense Gas Relative to Air 17
3.3. CO_2 Changes Phase over Commonly Encountered P-T Ranges 17
3.4. Joule-Thomson Cooling 18
3.5. Jet-Mixing Effect 19
3.6. Effects of Direction of the Leak with Respect to Horizontal 21
3.6.1. Upward Leak 21
3.6.2. Downward Leak 22
3.6.3. Horizontal Leak 23
3.7. Effect of Velocity of the Jet Flow 24
4. Pipeline Failure Hazards 26
4.1. Hazards of High-Pressure CO_2 Pipeline Leakage 26
4.2. Shock Wave Generated by the Sudden Expansion of the Gas 27
4.3. Failure Frequency Analysis 28
5. Quantifying and Displaying CO_2 Pipeline Leakage Risk 31
5.1. Threshold Concentrations and Consequence Proxy 31
5.2. Risk Communication 32
6. Description of CO_2 Transportation Within the ADM Plant 33
6.1. CO_2 Transportation, Flow Rate and Pipeline Geometries 33
6.2. The ADM Plant 34
6.3. Meteorological Characteristics 35
7. Modeling Approach 37
7.1. Building the Model System 37

7.2. Wind Field ... 40
8. Pipeline Failure Scenarios ... 44
8.1. Leakage Locations ... 44
8.2. Source Strength Evolution: Pipe Decompression Model ... 45
9. Atmospheric Dispersion of CO_2 Within the Plant and Assessment of Risks ... 51
9.1. Introduction ... 51
9.2. Pipeline route ... 51
9.3. Leakage and Dispersion ... 54
9.4. Scenario 1 ... 56
9.5. Scenario 2 ... 60
9.6. Scenario 3 ... 64
9.7. Scenario 4 ... 68
9.8. Pressure Blast Exposure Risk ... 71
10. Discussion ... 73
11. Recommendations ... 76
12. Conclusions ... 79
13. References ... 81
Appendix A. Experience with Pipeline Transportation of CO_2 ... 86
A.1. Seismic hazard for pipeline systems ... 88
Appendix B. Pipe decompression model ... 90
Appendix C. Fluidyn PANACHE, model description ... 93
C.1. Navier-Stokes Equations ... 93
C.2. Turbulence models ... 95
C.3. Boundary conditions ... 96
C.4. Site data incorporation by PANACHE ... 97
C.4.1. Terrain characteristics ... 97
C.4.2. Meteorological inputs ... 98
C.5. PANACHE. Validation and verification ... 100

List of Figures

Figure 1. CO_2 phase diagram (Pasquetto and Patrone, 1994). 18

Figure 2. Schematic view of two-phase jet release from the TNO manual on Risk of Gas Transportation (so-called Yellow book) (TNO, 1996). 20

Figure 3. CO_2 release experiment at Dordrecht, Netherlands, by Shell (Kuipjer, 2008). The image shows how the solid CO_2 (dry ice) is entirely reconverted to gas for vertical leaks. 22

Figure 4. A dry-ice bank is being formed from the downward release of CO_2 from a high pressure container (Mazzoldi et al., 2007). 23

Figure 5. Overhead view of the ADM plant, Decatur, IL. The pipeline transporting CO_2 is shown on the map by the red line. The flow of CO_2 in the pipeline is from south to north. 34

Figure 6. Average yearly wind directions and speed in Springfield, IL. 36

Figure 7. ADM's built environment as implemented in PANACHE. The gray shapes with red-borders are three-dimensional buildings and other flow obstacles considered by the model. 38

Figure 8. Oblique view of the ADM plant with major buildings as implemented in the model. The orange background represents a surface with roughness corresponding to an urban environment with buildings of height 5 m, the green color represents grassy field, and the dark green is forest. Some of the ground surface (black in the figure) was left without a specific roughness for better resolution when considering plumes of different gas concentrations. The dark red line is the pipeline. 39

Figure 9. Wind fields before the beginning of the jet release for Scenarios 3 (a) and 2 (b) (see below). Note the southeastern-most tank has been left out because it would

have crossed the boundary of the nasted domain, much affecting the creation of the mesh 41

Figure 10. Wind velocity vectors 15 s after the start of the CO_2 release for Scenarios 3 (a) and 2 (b). The high-speed of the CO_2 leak prevents display of the natural wind around buildings when consistent scaling of wind velocity vectors is used. 43

Figure 11. Route of the pipeline (red line) from the capture/compression facility (south) to the injection well (north). In green are displayed the railway lines within the plant..... 44

Figure 12. Model full-bore leakage-rate evolution in time. The black line represents the release rate along time as modeled by the Pipe model, for the 1 km scenario (Source A). Flow rates have been discretized into six steps of constant release for input into PANACHE (red line). The violet line is the release calculated with the Wilson model (not used here), and the green line represents the velocity of the gas exiting through the broken end of the pipe with time. 48

Figure 13. Model full-bore release rates and exit velocity as a function of time. The black line represents the release rate modeled by the Pipe model, for the 500 m scenario. Leakage rates have been discretized into five steps of constant release within PANACHE (red line). The violet line is the release calculated with the Wilson model (not used here), and the green line represents the velocity of the gas exiting through the broken end of the pipe. 49

Figure 14. Overhead view of the plant with leakage locations of Scenarios 1-4 indicated. The pipeline is elevated several meters above ground to pass over the railroad tracks at the location of the green circle. 52

Figure 15. The capture and compression station at the ADM plant. 53

Figure 16. Pipeline route (thick dark red line) and areas where CO_2 dispersion is considered in the following simulations. 55

Figure 17. Simulation results for Scenario 1. (a) Wind velocity field in the area of dispersion as modified by the presence of buildings. (b) Oblique view of the model plant showing results at t = 90 s of the 100,000 ppm contour surface (blue region near leakage source), 40,000 ppm isosurface (white surface), and 10,000 ppm and lower color contours on the ground surface. The red surface representing 250,000 ppm is very small and not visible in this figure. 57

Figure 18. Simulation results showing the CO_2 isoconcentration lines (see text) at eight times following the start of the leak for Scenario 1. 59

Figure 19. Simulation results for Scenario 2. (a) Wind velocity field in the area of dispersion as modified by the presence of buildings. (b) Oblique view of the model plant showing results at t = 130 s of the 100,000 ppm contour surface (blue region near leakage source), 40,000 ppm isosurface (white surface), and 10,000 ppm and lower color contours on the ground surface. The red surface representing 250,000 ppm is very small and not visible in this figure. 61

Figure 20. Simulation results showing the CO_2 concentration isopleths (see text) at eight times following the start of the leak for Scenario 2. 63

Figure 21. Simulation results for Scenario 3. (a) Wind velocity field in the area of dispersion as modified by the presence of buildings. (b) Oblique view of the model plant showing results at t = 190 s of the 100,000 ppm contour surface (blue region near leakage source), 40,000 ppm isosurface (white surface), and 10,000 ppm and lower color contours on the ground surface. The red surface representing 250,000 ppm is visible near the rupture point..... 65

Figure 22. Simulation results showing the CO_2 concentration isopleths (see text) at eight times following the start of the leak for Scenario 3. 67

Figure 23. Simulation results for Scenario 4. (a) Wind velocity field in the area of dispersion as modified by the presence of buildings. (b) Oblique view of the model plant showing results at t = 150 s of the 250,000 ppm contour surface (red region near source), the 100,000 ppm contour surface (blue region), 40,000 ppm

isosurface (white surface), and 10,000 ppm and lower color contours on the ground surface. 69

Figure 24. Simulation results showing the CO_2 concentration isopleths (see text) at eight times following the start of the leak for Scenario 4. 70

Figure C1. Locations of five arcs (x = 50, 100, 200, 400, and 800 m) in the Prairie Grass experiment (Barad, 1958). 100

List of Tables

Table 1. Yearly failure rate summary per module (Vendrig et al., 2003)..... 29

Table 2. Expected failure rate (event per year per module) for give sizes of leakage for each of the five Modules in Table 1 (Vendrig et al., 2003). 30

Tables 3A and 3B. Transportation system characteristics and leakages details. 47

Table 4. Effects of characteristic pressure pulses on humans. Also, the maximum distance of fatal pressure blasts for pipes studied in the EI report are shown (689 mbar = 0.0689 MPa)..... 71

Acronyms

2D, 3D	Two-dimensional, Three-dimensional
ADM	Archer Daniels Midland
CCS	Carbon Capture and Storage
CFD	Computational Fluid Dynamics
CO_2	Carbon Dioxide
CV	Control Volume
DNV	Det Norske Veritas
EI	Energy Institute
EOR	Enhanced Oil Recovery
EOS	Equation of State
ESD	Emergency Shutoff Device
HP	High Pressure
IBDP	Illinois Basin Decatur Project
IDLH	Immediately Dangerous to Life and Health
J-T	Joule-Thomson
NIOSH	National Institute for Occupational Safety and Health
PBL	Planetary Boundary Layer
TNT	Trinitrotoluene

Abstract

The Illinois Basin Decatur Project (IBDP) is designed to confirm the ability of the Mt. Simon Sandstone, a major regional saline-water-bearing formation in the Illinois Basin, to store 1 million tons of carbon dioxide (CO_2) injected over a period of three years. The CO_2 will be provided by Archer Daniels Midland (ADM) from its Decatur, Illinois, ethanol plant. In order to transport CO_2 from the capture facility to the injection well (also located within the ADM plant boundaries), a high-pressure pipeline of length 3,200 ft (975 m) has been constructed, running above the ground surface within the ADM plant footprint. We have qualitatively evaluated risks associated with possible pipeline failure scenarios that lead to discharge of CO_2 within the real-world environment of the ADM plant in which there are often workers and visitors in the vicinity of the pipeline.

There are several aspects of CO_2 that make its transportation and potential leakage somewhat different from other substances, most notable is its non-flammability and propensity to change to solid (dry ice) upon strong decompression. In this study, we present numerical simulations using Computational Fluid Dynamics (CFD) methods of the release and dispersion of CO_2 from individual hypothetical pipeline failures (i.e., leaks). Failure frequency of the various components of a pipeline transportation system over time are taken from prior work on general pipeline safety and leakage modeling and suggest a 4.65% chance of some kind of pipeline failure over the three-years of operation. Following the Precautionary Principle (see below), we accounted for full-bore leakage scenarios, where the temporal evolution of the mass release rate from the high-pressure pipeline leak locations was simulated using a state-of-the-art Pipe model which considers the thermodynamic effects of decompression in the entire pipeline. Failures have been simulated at four representative locations along the pipeline route within the ADM

plant. Leakage scenarios at sites along the route of the pipeline, where plant operations (e.g., vehicular and train transportation) seem to present a higher likelihood of accidental failure, for example due to vehicles or equipment crashing into the pipeline and completely severing it, were modeled by allowing them to have a double source consistent with the pipeline releasing high-pressure CO_2 from both ends of the broken pipe after a full-bore offset rupture.

Simulation results show that the built environment of the plant plays a significant role in the dispersion of the gas as leaking CO_2 can impinge upon buildings and other infrastructure. In all scenarios simulated, the region of very high-concentration of CO_2 is limited to a small area around the pipeline failure, suggesting the likelihood of widespread harmful CO_2 exposure to plant personnel from pipeline leakage is low. An additional risk is posed by the blast wave that emanates from a high-pressure pipeline when it is breached quickly. We estimate the blast wave risk as low because it occurs only for a short time in the immediate vicinity of the rupture, and requires an instantaneous large-scale rupture to occur.

We recommend consideration of signage and guard rails and posts to mitigate the likelihood of vehicles crashing into the pipeline. A standardized emergency response plan applicable to capture plants within industrial sites could be developed based on the IBDP that would be useful for other capture plants. Finally, we recommend carrying out coupled wellbore-reservoir blowout scenario modeling to understand the potential for hazardous conditions arising from an unexpected blowout at the wellhead.

1. Introduction

We have carried out pipeline leakage risk assessment for the 3,200-ft (975-m) by 6-in (15-cm) diameter pipeline that will transport carbon dioxide (CO_2) at pressures of approximately 1,400 psi (10 MPa) from the capture facility at the Archer Daniels Midland (ADM) ethanol plant in Decatur, Illinois, to the well that will be used to inject CO_2 into the Mt. Simon saline aquifer at a depth of 7,000 ft (2,100 m). The approach used is numerical modeling of dense gas dispersion for assumed pipeline leakage scenarios at the ADM plant site. The principal consequences of a high-pressure leak of CO_2 into the environment is the possibility for asphyxiation of by-standers in the close vicinity of the leak as CO_2 is hazardous at high concentrations in air (>10% by volume) and rapidly fatal at very high concentrations (>25%). The results of the modeling comprise figures and maps of spatial and temporal CO_2 concentrations above threshold values. In this report, we describe the risk analysis approach, some special considerations critical to risk assessment of CO_2 pipeline leakage, and present results of scenario analysis and transient numerical simulations of dispersing CO_2 plumes. In addition to modeling new scenarios relative to our earlier report (Mazzoldi and Oldenburg, 2011), we have improved our simulations by the use of an advanced model for the source term for the atmospheric dispersion model, namely the time-dependent release rate appropriate for a ruptured high-pressure pipeline (Picard and Bishnoi, 1988). Rather than referring repeatedly to the earlier report, we have duplicated some material from Mazzoldi and Oldenburg, (2011) to make this report comprehensive.

The presentation begins with a review of pipeline risk assessment including discussion of the unique aspects of CO_2 leakage, followed by description of the modeling approach we have used. The main results of the modeling are presented through figures showing the extent and geometry of simulated threshold contours of CO_2 concentrations. Appendix A provides background

information and references on experience with transporting CO_2 by pipeline. Appendix B describes state-of-the-art numerical methods used for modeling the depressurization process of the high pressure pipeline (Pipe model) developed by D. Picard (Picard and Bishnoi, 1988), while Appendix C provides information on the CFD model Fluidyn PANACHE that was used for the atmospheric dispersion simulations.

Disclaimer

While care has been taken to ensure accuracy and relevance, this document is not and does not purport to be comprehensive or to contain all of the information that readers may require. Accordingly, LBNL, its sponsors, the Regents of the University of California and authors cannot accept any responsibility for any inaccuracy or omission or action taken, or not taken, on the basis of this information. LBNL and the contributors do not make any representation or warranty in respect to the information contained in this document and shall not be liable to any person for any loss or damage which may arise from the use of any of the information contained herein.

2. Risk Assessment for CO_2 Pipeline Leakage

In general, the quantification of risk involves estimating the product of the frequency of occurrence of a hazardous event times the potential consequences of that event (Engebo et al., 2007). Hence, in order to determine the risk there are three discrete sets of information that need to be developed, namely

- Identification of hazards;
- Frequency of occurrence (likelihood) of scenarios involving hazards;
- Consequences of the scenarios occurring.

In the case of CO_2 transportation in high-pressure pipelines, the main hazard is that leakage could give rise to CO_2 gas plumes at concentrations above acceptable limits that could cause acute health effects including asphyxiation. For high-pressure pipelines, the failure probability of some parts of the high-pressure transportation system has been well documented in the oil industry literature (Burgherr and Hirschberg, 2005; Hirschberg et al., 2004; Townes et al., 2004) and the principal failure modes of natural gas/CO_2 pipeline incidents have been classified. These principal modes are: relief valve failure, weld/gasket/valve packing failure, corrosion, and outside forces (vehicle collisions, penetrations, support collapse, and seismicity).

Vendrig et al. (2003) estimated an overall failure frequency or likelihood from a generic Carbon Capture and Storage (CCS) transportation system of about 0.32 yr^{-1}, irrespective of its location (under or above the ground surface) but with much higher likelihood of occurrence along parts of the system characteristically placed above the ground (see Section 4.3, Table 1). This likelihood applies at the source of the compressed gas (CO_2 capture facility), near the end of the transportation pipeline (at the injection facility), and at pressure-booster stations along the pipeline route, while it is generally lower along other regions of a pipeline. This failure

frequency includes every kind of failure including the most frequent and inconsequential leakage events.

The relatively high failure likelihood does not equate to high leakage risk because the consequences of common failures are negligible, e.g., frequent minor and short-lived leaks cause no measurable harm. Nevertheless, some leakage scenarios involving CO_2 could have serious consequences in certain circumstances, also because CO_2 is a dense gas that may persist at the ground surface rather than rise upwards and quickly dissipate (IEA, 2009). These high-consequence events motivate the need for CO_2 pipeline leakage risk assessment.

Depending on the pipeline pressure, the size of the opening through which leakage occurs, and whether or not the section of the pipeline or facility involved in the leakage is buried or above ground, hugely varying amounts of CO_2 can be released to the atmosphere with very different hazards to people and the environment in the proximity of the release. The plume formed by a high-pressure release will be controlled by (1) the time-varying decrease in release rate from the pipeline (as the in-pipeline pressure decreases), and (2) the atmospheric conditions (stability, wind speed and direction, turbulence, pressure and temperature) and (3) site topography (including the presence or absence of buildings, walls, etc.). These factors influence the development of the plume and, therefore, its hazard.

This report considers CO_2 plumes of hazardous concentrations and their development over short time-scales due to potential failures of the CO_2 transportation system within the ADM plant. In order to have a clearer view of the potential hazard faced by people present in areas intersected by a potential high-pressure release of supercritical CO_2 that transforms into a heavy CO_2 cloud, we use the CFD approach. We model how the presence of buildings and other obstructions can

affect the atmospheric concentrations of the released gas as it moves due to the high pressure release, and gravitational and ambient-wind forcing.

3. Special Considerations for CO_2 Leakage and Atmospheric Dispersion

3.1. Effects of CO_2 on Humans

Carbon dioxide is an odorless colorless gas that occurs naturally in the atmosphere and is produced by the human body during ordinary respiration. It is commonly perceived by the general public to be a relatively harmless gas. However, although the Immediately Dangerous to Life and Health (IDLH) limit set by the National Institute for Occupational Safety and Health (NIOSH) is 40,000 ppm (4%), at concentrations above 10% by volume (100,000 ppm), CO_2 may cause unconsciousness after a few minutes and is potentially fatal after 15 minutes of continuous inhalation (Vendrig et al., 2003). At concentrations above 25% (250,000 ppm) it poses a significant asphyxiation hazard (Parfomak and Folger, 2008) and could impede the ability of a person to move after a few breaths and lead to death in about one minute (Doss et al., 1993).

3.2. CO_2 is a Dense Gas Relative to Air

Carbon dioxide (CO_2) at typical ground-surface *P-T* conditions (1,000 hPa and 20 °C) is a dense gas relative to air (ρ_{CO2} = 1.8 kg m^{-3}, ρ_{air} = 1.2 kg m^{-3}). Air-CO_2 mixtures with CO_2 at concentrations higher than a certain value (usually taken as 10,000 ppm) (Kruse and Tekiela, 1996) will tend to remain near the ground, filling topographic lows and valley floors. At low concentrations, CO_2 will be diluted in air and behave as a passive (no density effect) gas component in the air mixture (Oldenburg, 2007; Oldenburg and Unger, 2004).

3.3. CO_2 Changes Phase over Commonly Encountered P-T Ranges

There are four different phase states for CO_2, i.e., solid, gas, liquid, and supercritical. The phase diagram in Figure 1 shows the boundaries between these phases and the coordinates of some relevant points. Above the critical pressure of 1,090 psi (7.4 MPa) and at temperatures higher

than 31 °C (88 °F), CO_2 is in its supercritical form. In this form, CO_2 has a liquid-like density but also behaves as a gas, i.e., its viscosity is low and it occupies the volume of its container (Pasquetto and Patrone, 1994). This behavior demonstrates that CO_2 is a highly non-ideal gas, i.e., its thermodynamic properties are not well described by the ideal gas law ($PV = nRT$).

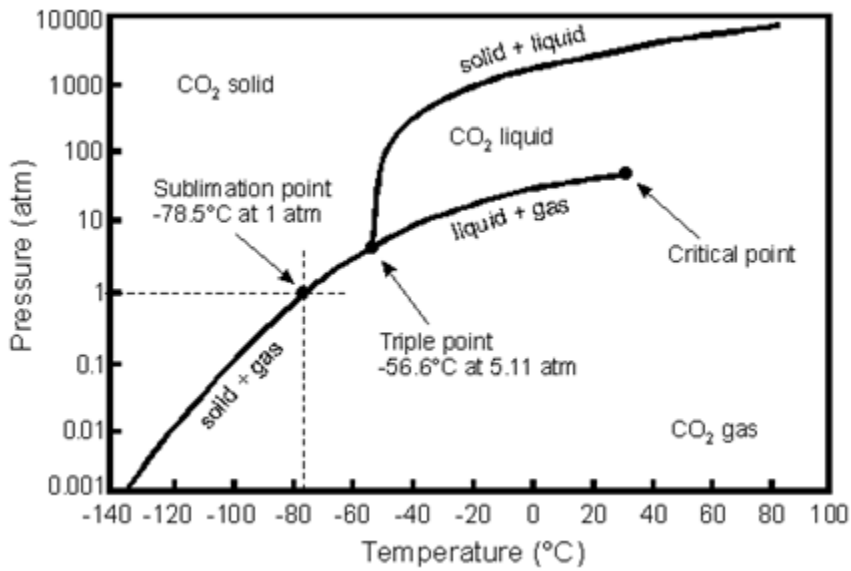

Figure 1. CO_2 phase diagram (Pasquetto and Patrone, 1994).

3.4. Joule-Thomson Cooling

When CO_2 (or any gas) expands adiabatically (no heat transfer to its surroundings), the temperature changes. For most common gases at near-ambient conditions, temperature decreases with pressure, the so-called Joule-Thomson cooling effect. The Joule-Thomson effect can be described by the equation

$$\Delta T = \varphi \cdot \Delta P \qquad (1)$$

where φ is the Joule-Thomson (J-T) coefficient. For CO_2, the value of the J-T coefficient (φ_{CO2}) is approximately 13 K MPa^{-1} (Atkins, 2010). From Equation 1, we note that the temperature drop caused by the pressure change of 1,470 psi (10 MPa) after leakage from a CO_2 pipeline at 25 °C

into the atmosphere (P = 1 bar or 0.1 MPa) would be approximately 130 °C (234 °F). Figure 1 shows that when CO_2 decompresses from 10 MPa to 0.1 MPa with an associated 130 °C temperature drop, the CO_2 will change phase from liquid to solid state (dry ice).

Below –78.8° C at 0.1 MPa, CO_2 is in a solid state (also known as 'dry ice') with a density of 1,562 kg m^{-3}. At a temperature slightly higher than the sublimation temperature, gaseous CO_2 has a density of about 2.8 kg m^{-3}, significantly higher than its value at standard conditions of 0.1 MPa, 20 °C (14.7 psi, 68 °F) of approximately 1.8 kg m^{-3} (Mazzoldi et al., 2007). The simultaneous presence of dry ice and very cold gaseous CO_2 formed after a high-pressure pipeline release increases the tendency of CO_2 to stay near the ground, hence enhancing its asphyxiation hazard.

3.5. Jet-Mixing Effect

As it leaks from a high pressure (HP) facility, a fluid can only exit the container at a speed less or equal to the speed of sound in the fluid, at the temperature and pressure conditions encountered in the fluid exiting the facility (Kuprewicz, 2007). Near the source at sonic speed, the very large amount of leaking fluid would find it difficult to expand instantaneously to atmospheric pressure[1], but will instead start to mix with ambient air. As the jet flow expands with distance away from the leak, it decreases in velocity and increases the rate of entrainment of ambient air (Wakes et al., 2002). This mixing is mainly governed by the difference in velocity between the CO_2-jet and air and the consequent strong initial resistance imposed by air to the flow of the jet (Figure 2), providing heat for the reconversion of dry ice into cold gas. The jet effect, which is due to the difference in physical properties of the two substances (density, temperature, and

[1] as it will be seen below, this will cause, soon after the start of the leak, the formation of a pressure blast front which can be deadly up to some meters away from the leak (EI, 2010).

momentum), extends the region of high CO_2-gas concentrations in the ambient air, away from the source.

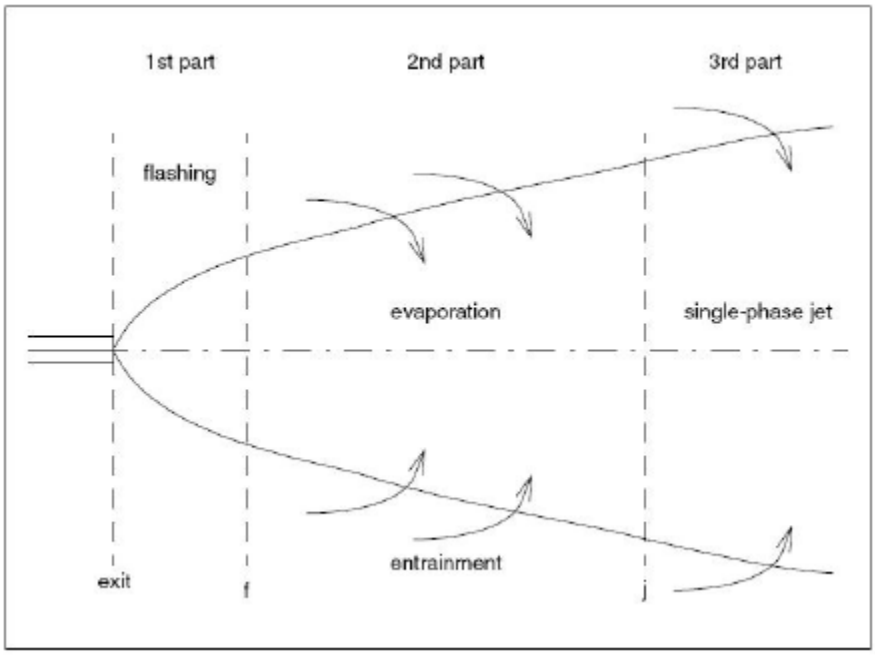

Figure 2. Schematic view of two-phase jet release from the TNO manual on Risk of Gas Transportation (so-called Yellow book) (TNO, 1996).

Figure 2 shows that a two-phase jet flow is generally composed of three parts. Specifically for CO_2, in the first part, the CO_2 molecules freeze into dry ice after expansion by the Joule-Thomson effect. In the second part, the flow is extremely turbulent and molecules sublime back to gas, due to frictional heating between jet and air, as entrainment and mixing become predominant. Some of the dry ice droplets may not reconvert to the gaseous state, and are subject to rain-out of the jet flow, falling to the ground. In the third phase, all the molecules composing the flow are in the gaseous phase and the jet continues its expansion with even more air entrainment. At some distance, the jet will stop, allowing dispersion and dilution in air controlled by density effects and ambient wind. The behavior of the jet is also a function of its direction (upward, sideways, or downward) relative to the pipe, as detailed below.

3.6. Effects of Direction of the Leak with Respect to Horizontal

Depending on the direction of the fast moving jet relative to the horizontal, different aspects of the flow process will control the development of the release after expansion. Below, three scenarios are considered.

3.6.1. Upward Leak

In Figure 3 an upward leak of CO_2 from a container under pressure is shown. The white color of the jet occurs because the CO_2 rapidly decompresses and cools forming dry ice, also condensing water from entrained ambient air and solidifying it to ice (compare Figure 3 with Figure 2). The frictional heating of the jet in the air may provide enough energy for the dry ice (formed due to the Joule-Thomson effect) to sublimate back into gas (Mazzoldi, 2009).

Figure 3. CO_2 release experiment at Dordrecht, Netherlands, by Shell (Kuipjer, 2008). The comparison of the image with Figure 2 can be of help in understanding the evolution of the CO_2 dispersion away from the high-pressure source.

3.6.2. Downward Leak

In the case of a downward-directed leak from an above-ground pipeline, the jet flow of CO_2 impinges on the ground without reconverting to gas. The result is that a bank of dry ice forms on the ground, growing with time as the leak continues. Figure 4a shows an example of a downward CO_2 release from a high-pressure container and the resulting dry-ice bank formation. The subsequent sublimation of CO_2 from a dry-ice bank does not appear to pose an immediate risk for people in the vicinity of the bank because the rate of sublimation of gaseous CO_2 is sufficiently slow that CO_2 concentrations in air only reach dangerous levels at very low wind speeds, as shown in Figure 4b (Mazzoldi et al., 2007).

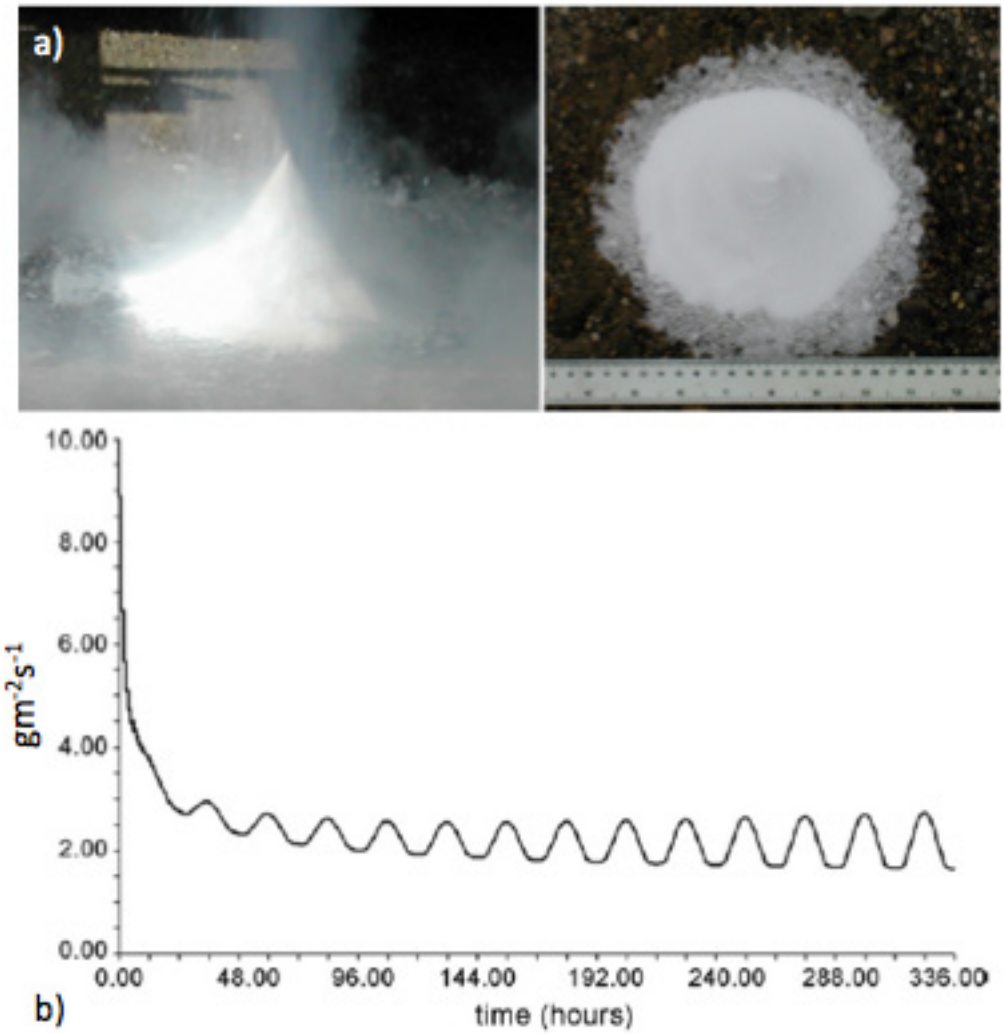

Figure 4. a) A dry-ice bank is being formed from the downward release of CO_2 from a high pressure container; b) The consequent sublimation of solid CO_2 from the bank surface does not allow the formation of high concentrations of the gas in air.

3.6.3. Horizontal Leak

If a nearly horizontal leak develops from a high pressure pipeline or tank, the cloud will develop primarily horizontally, posing the highest hazard to people in the vicinity of the failure. Some dry ice may drop out from the jet flow and remain on the ground until it sublimates again, representing a minor additional potential source of CO_2. Given the difficulty of evaluating the

amount of dry ice falling on the ground over time and for different angles formed by the jet flow with the horizontal, in the reminder of this document we assume that no dry ice drops out of the flow. This assumption is conservative in that more CO_2 will be present in the flowing jet and plume, which are considered the main hazard associated with high-pressure CO_2 leakage.

The exact shape of the plume formed as a result of a nearly horizontal high-pressure release is strongly dependent on the environment in which the release takes place. For example, in the presence of buildings or other obstructions, the dispersing gas will tend to fill the space between them. The shape of the plume would also be influenced by the wind near the ground, which is also influenced by the shape, size, orientation, and density of buildings and other obstructions. Due to these effects and to the higher overall risk posed by pipelines when they are located above ground and close to vehicles, workers and visitors, it is critical to model the details of dispersion of CO_2 leakage by CFD methods rather than by the Gaussian dispersion approach. A comparison between the two approaches, with an analysis of the differences and a statement for a need of change in Risk Assessment drafting is provided in Mazzoldi et al., 2008, 2011 and 2012.

3.7. Effect of Velocity of the Jet Flow

The velocity of the CO_2 gas, as it leaks out of the pipe, is the main factor influencing the degree of mixing of the gas with air, and hence the hazards associated with high concentrations. When the speed of the gas ejected into the atmosphere from the high-pressure pipeline is choked (cannot increase over a certain value), it is flowing at the speed of sound in the fluid at those conditions (of P and T) (Perry et al., 1984). This speed is usually calculated as $c = \sqrt{\frac{C}{\rho}}$ (Perry et al., 1984), where C is the modulus of bulk elasticity for the gas medium and ρ is the density of the fluid exiting from the pipe. The pipe outflow model (Appendix B) we are using for

estimating release-rate variation over time can evaluate the density of the fluid in the section of the pipeline experiencing quick pressure decrease. This allows estimation of the speed of sound and hence the velocity of the fluid across the leak in choked conditions. The pipe outflow model is a significant improvement over the standard approach we used previously (Eq. 2, Mazzoldi and Oldenburg, 2011).

4. Pipeline Failure Hazards

4.1. Hazards of High-Pressure CO_2 Pipeline Leakage

The first step in risk assessment in the context of hazardous material transport in pipelines is to identify the potential scenarios (e.g., accidents) that could result in the release of the hazardous material, in this case CO_2, its direct effects on humans and other animals, along with the associated potentially damaging effects such as noise and physical injuries, (e.g., from flying debris), and their probability of occurrence.

The modular approach to engineered transportation systems is based on components such as pipes and fittings, equipment such as compressors, and storage vessels such as tanks. Process failure data for pipeline systems are well-established. Failure rate data are available to define representative accident scenarios for all of the generic items included in the modular system. These hazards of the engineered system include failures caused by mechanisms such as corrosion, vibration, or external impacts, and apply to components including the following: pipelines (buried and surface), flanges, valves, fittings, pressure vessels, pumps and compressors. The range of possible releases for a given component covers a broad spectrum, from a pinhole leak up to a catastrophic pipe or vessel rupture. For risk assessment, it is not necessary to consider every part of the system; instead, representative failure scenarios can be considered. To accomplish this, statistical data from the oil transportation industry during the last 50 years are taken from the work of Det Norske Veritas (DNV) to establish likelihoods of various failure scenarios (Vendrig et al., 2003). In their report they considered four different representative leak sizes along with their expected failure frequencies or likelihoods, showing results for the subsequent atmospheric dispersion of the gas obtained by Gaussian simulation.

Setting scenarios that reflect the range of loss of containment issues that might occur is crucial to evaluating the hazard. An incident involving loss of containment from a high-pressure CO_2 facility or pipeline may result in the release of a gas cloud along with an uncontrollable release of energy. There are significant health and safety hazards associated with (1) potential inhalation of the gas at high concentrations, (2) the impact of the local shock wave in the air formed by the sudden pressure drop in the pipeline and associated gas release (EI, 2010), (3) potentials for flying objects thrown by the blast, and (4) the low temperatures developed in proximity of the release source.

Damage to adjacent equipment, structures (such as buildings), and the environment needs also be considered where appropriate, especially if this damage can cause further hazardous events such as fires or explosions, release of stored material, falling objects, or flying blast-fragments. Failures in containment can range from small, transient leaks through to large-scale pipe ruptures, and the consequences may vary from inconsequential or reversible health effects to fatal or serious injury, and major economic losses. As will be discussed below, in order to make conservative predictions, all releases considered in this report have a source with dimensions equal to the cross-section of the pipe, i.e., full-bore leaks over the full 6 inch (15 cm) pipe' cross section.

4.2. Shock Wave Generated by the Sudden Expansion of the Gas

The hazard arising from the shock wave generated from catastrophic ruptures of high-pressure pipelines deserves extra comment. The velocity of the escaping gas from the pipeline is limited to its speed of sound in choked conditions. The actual release velocity just downstream from the rupture is equal to the speed of sound plus the speed of the gas particles driven by the rapid

expansion into ambient air. In this extremely fast process, pressure gradients do not have the time to develop and the energy is dissipated through the creation of a spherical pressure front that expands radially from the broken end of the pipe (Schardin, 1954; Stoner and Bleakney, 1948). This sudden expansion is analogous to a blast-front (the front of the shock-wave) caused, for instance, by an explosion of Trinitrotoluene (TNT). The energy generated by the explosion can be estimated by comparing the actual effects of the explosion (or the measured blast-front amplitudes at given distances from the detonation center) with the experimentally measured effects (or blast-front amplitudes) of determined masses of TNT charges (Kleine et al., 2003). The dissipation in space of the pressure blast will be approximately linear with distance from the breach and dependent on the energy of the initial shock front. The pressure blast front, while short-lived (hundredths of a second) and limited in space to the immediate vicinity (on the order of meters) of the catastrophic rupture, can be fatal to anyone in its path.

4.3. Failure Frequency Analysis

Defining the failure hazard in terms of probability requires an estimate of the expected frequency of occurrence of the failure. Here, "failure" is defined as any unwanted event that prevents the transportation system from working correctly and which causes a leak of the substance transported. Estimating this expected frequency is usually done based on historical data taken from the field of pipeline fluid transportation, in particular for hydrocarbons. We use data from the work of DNV (Vendrig et al., 2003) who classified this frequency on the basis of individual modules comprising the transportation system. These are widely considered to be the best available data and to be applicable to pipes and equipment carrying CO_2 (Mazzoldi et al., 2011). Table 1 gives a summary of failure rates per year, for each module of a pipeline transportation

system, considering leakages of any possible dimension (from very small openings to full-bore ruptures).

Table 1. Average yearly failure rate summary per module (Vendrig et al., 2003).

Module		**Expected failure rate (events per module per year)**	**Leak every x years**
1	CO_2 recovery at source	$1.5 * 10^{-1}$	7
2	Converging pipelines	$4.6 * 10^{-3}$	217
3	Booster station	$4.0 * 10^{-2}$	25
4	10 km pipeline	$3.4 * 10^{-4}$	2,941
5	Injection well	$1.8 * 10^{-1}$	6

We note that the failure frequency of Vendrig et al. (2003) includes the length of pipeline directly associated with each module of the pipeline system (see Table 1). Of the five modules considered in Table 1, only Modules 1, 4, and 5 will be accounted for in the present study because the IBDP pipeline will not have converging pipelines nor booster stations. The length of the pipeline at the ADM plant is in fact relatively short and the pipeline used for carrying the gas is not expected to face problems of pressure drop, generally caused by pipe-wall drag on the fluid or significant changes in elevation over long distances.

Table 2 classifies the expected failure rates associated with each module by the representative leak size. The frequency broadly decreases with the leak size. We note that full-bore failures are significantly more frequent than large failures, while the area intersected by the event and the associated consequences presumably increase with leak size.

Table 2. Expected failure rate (event per year per module) for given sizes of leakage for each of the five Modules in Table 1 (Vendrig et al., 2003).

Module	Small (3-10 mm)	Medium (10-50 mm)	Large (50-150 mm)	Full-bore (>150 mm)
1	$9.6 * 10^{-2}$	$5.1 * 10^{-2}$	$2.0 * 10^{-3}$	$5.6 * 10^{-3}$
2	$3.5 * 10^{-3}$	$8.8 * 10^{-4}$	$1.0 * 10^{-4}$	$1.5 * 10^{-4}$
3	$3.5 * 10^{-2}$	$3.8 * 10^{-3}$	$3.0 * 10^{-4}$	$8.8 * 10^{-4}$
4	$1.4 * 10^{-4}$	$9.5 * 10^{-5}$	$2.0 * 10^{-5}$	$8.5 * 10^{-5}$
5	$1.2 * 10^{-1}$	$5.3 * 10^{-2}$	$2.1 * 10^{-3}$	$5.8 * 10^{-3}$

As stated above, only full-bore leaks are accounted for in the current study. It should be noted that the large leak in the DNV classification is up to 150 mm (15 cm) which is the diameter of the pipeline of the IBDP site, so effectively corresponds to a complete failure (i.e., full-bore leak). Accordingly, in our case study and assuming this statistical likelihood of Table 2 is applicable, there would be $(2 + 5.6 + 0.0 + 0.0 + 2.1 + 5.8) \times 10^{-3}$ per yr × 3 yr (large + full-bore leaks per year of modules 1, 4, and 5 over three years). That is, there would be a 4.65×10^{-2} or 4.65% probability of a full-bore failure over the three-year period of expected operation of the pipeline.

5. Quantifying and Displaying CO_2 Pipeline Leakage Risk

5.1. Threshold Concentrations and Consequence Proxy

This study considers the atmospheric dispersion of CO_2 after leakage from the pipeline transportation system at the ADM site, thereby indicating areas of hazard for people working in the plant. Results mainly consist of the evaluation of the extent of areas intersected by high concentrations of CO_2 for different pipeline failure scenarios. The concentration values considered are recognized as health-thresholds for CO_2 gas. Specifically, the following four threshold values are considered:

- 10,000 ppm. This value is the average of the long-term exposure limit (5,000 ppm for an 8-hour reference period in the UK) and short-term exposure limit (15,000 ppm for a 15-minute reference period in the UK);
- 40,000 ppm. IDLH (Immediately Dangerous to Life and Health) limit set by NIOSH;
- 100,000 ppm. The limit above which asphyxiation is likely to occur after 15 min of exposure;
- 250,000 ppm. Concentration that can cause unconsciousness after a few breath and consequent death (NIOSH).

The evolution with time of regions with concentrations at and above these threshold levels is assumed to be a good proxy for estimating consequences of the considered scenario. Indeed, a long-lived large CO_2 cloud with concentrations above 100,000 ppm (10% CO_2 by volume) may have serious consequences, whereas a shorter-lived smaller low-concentration cloud may have insignificant consequence. The concentration of 250,000 ppm, in the reminder of the report, is considered a deadly concentration. Without a model or data for the numbers and activities of people likely to be present at the time the pipeline ruptures, the actual potential exposure and

consequence to any particular individuals or average individuals cannot be calculated. Thus we use CO_2 concentration as a proxy for mapping the potential effects of the leak.

5.2. Risk Communication

The way in which results are presented is very important for risk communication. An effort has been made to present the results with figures that can be easily understood by workers and managers of the project. To show a dynamic process, such as the atmospheric dispersion of a gas, we use a time-series of images with the contours of the threshold concentrations described above. This is done at different positions along the pipeline route, while analyzing a variety of leakage scenarios (e.g., leakage of CO_2 near the compressor, near the injection well and at different positions along the pipeline, with settings characterized by buildings and structures within the plant).

6. Description of CO_2 Transportation Within the ADM Plant

6.1. CO_2 Transportation, Flow Rate and Pipeline Geometries

Injection in the IBDP project is planned to be approximately 1 million ton of CO_2 over a period of three years. This is equivalent to a continuous injection of about 10 kg s^{-1}, a rate which is the average flow rate through the pipe of diameter equal to 15.30 cm (6.025 in) ID and 16.83 cm (6.625 in) OD Schedule 40 pipe (Ray McKaskle, Trimeric, email of 12/2/10), which we approximate as 15 cm ID. The expected operating pressure of the pipeline is 1,400 psig which we approximate as 10 MPa, with a temperature of 35-43 °C (95-110 °F).

Shown in Figure 5 is an overhead view of a portion of the ADM ethanol plant with the IBDP transportation infrastructure superimposed. The pipeline is 975 m (3,200 ft) in length and runs from the dehydration station, which is within the heart of the ethanol plant, to the injection well which lies in an open field. Because the pipeline passes through the plant facility, there are numerous obstacles (buildings, roads, train tracks, etc.) that may allow for potential air stagnation, diminished dispersion, and increased risk. Because the pipeline length is only 975 m, there is no booster station nor Emergency Shutoff Devices (ESD valve) for closing-off segments of the pipe in case of unexpected leakage at some point along the route (Folga, 2007).

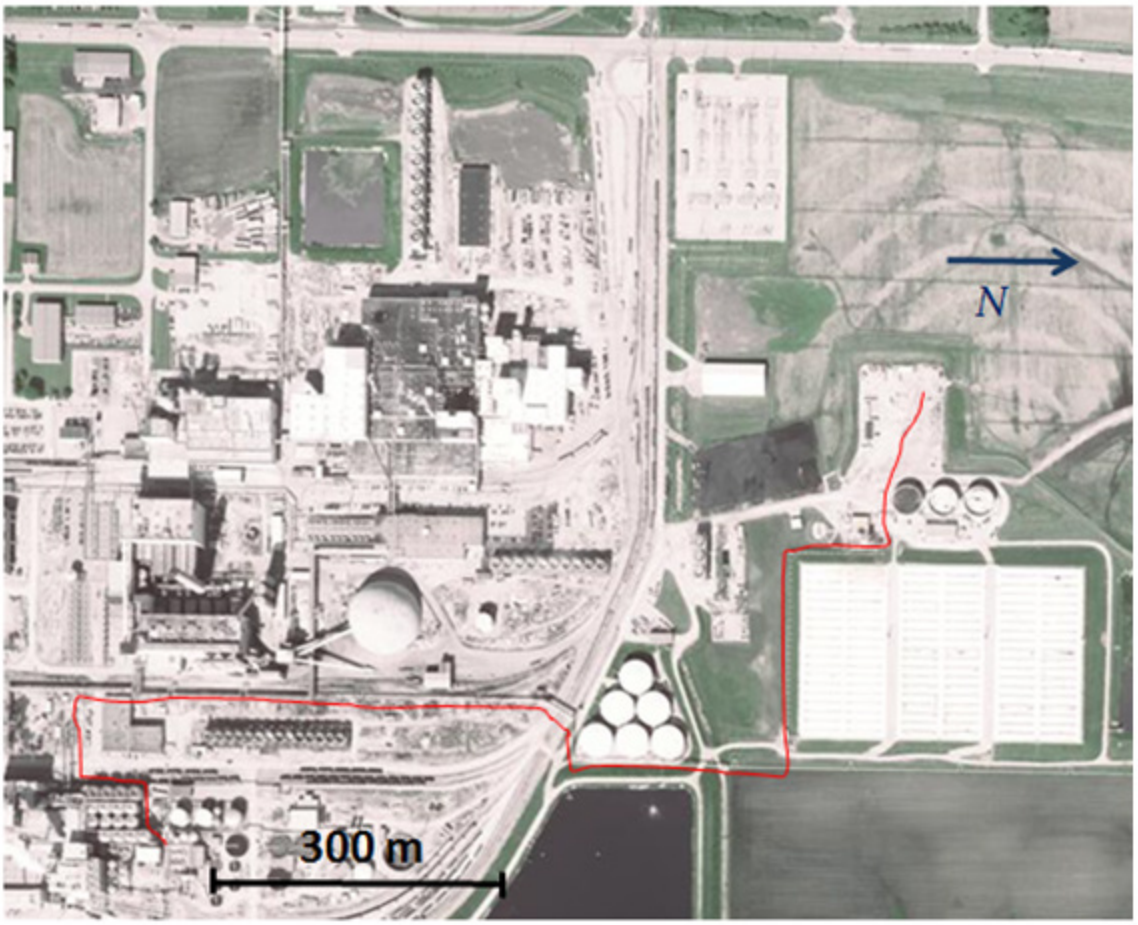

Figure 5. Overhead view of the ADM plant, Decatur, IL. The pipeline transporting CO_2 is shown on the map by the red line. The flow of CO_2 in the pipeline is from south to north.

6.2. The ADM Plant

The ADM industrial site is about 1.2 mi (2 km) in the N-S direction by 0.7 mi (1.2 km) in E-W direction. The area is occupied by buildings for the most part, with an open field on the northern side of the plant, where the injection well is located. At the Decatur site, many ADM employees spend part of their working time outside, in the open air.

Except around streams and lakes, the Decatur area is relatively flat as is the ground surface along the pipeline route. Detailed topographic maps show a 1.5 to 2.4 m (5 to 8 ft) ground elevation difference over the length of the pipeline.

The presence of buildings and other obstacles within the site is expected to produce a major effect on the dispersion of a dense gas such as CO_2, creating air-entrenchment zones were the gas could accumulate, creating a risk for workers. These effects are modeled in PANACHE through the placement of 3-D obstacles with shapes and dimensions equal to the actual buildings and structures found at the site of modeled potential failures.

6.3. Meteorological Characteristics

The city of Decatur, IL is characterized by a continental climate with warm summers and cold winters with variable humidity. Annual rainfall averages about 960 mm (38.3 in) with snowfall of about 510 mm (20 in). Average temperatures vary from a minimum of -7 °C (19 ^{o}F) in January to a maximum of 32 °C (89 ^{o}F) in July (e.g., http://illiniweather.com/cities/decatur.htm). Figure 6 shows a wind rose for the city of Springfield, 50 km west of Decatur. The relatively flat topography of the area allows us to take these data as characteristic also of the site under study. As shown in this Figure, winds blow mostly from the south with quite variable speed, averaging about 5-6 m s^{-1} (11-13 mph). In the simulations no preferential wind direction has been modeled. Instead, the wind direction was arbitrarily set in order to create wind re-circulations and interactions between the buildings for the various scenarios.

In order to make a detailed description of the proxy consequences, with the aim to be conservative, to ensure safety, consideration must be given to the effect of atmospheric conditions on plumes formed during the leakage events. In the results presented here, stable atmospheric conditions and slower wind speed are given priority because well-stratified and calm conditions tend to inhibit mixing and dispersion. Specifically, simulations performed in this study use atmospheric stability Classes E and F (Gifford, 1961; Pasquill, 1961, 1974). We note further that the buildings, characteristic of the industrial ADM plant, provides obstacle to air

flow that could increase the possibility of CO_2 accumulation and tend to prevent mixing and dispersion.

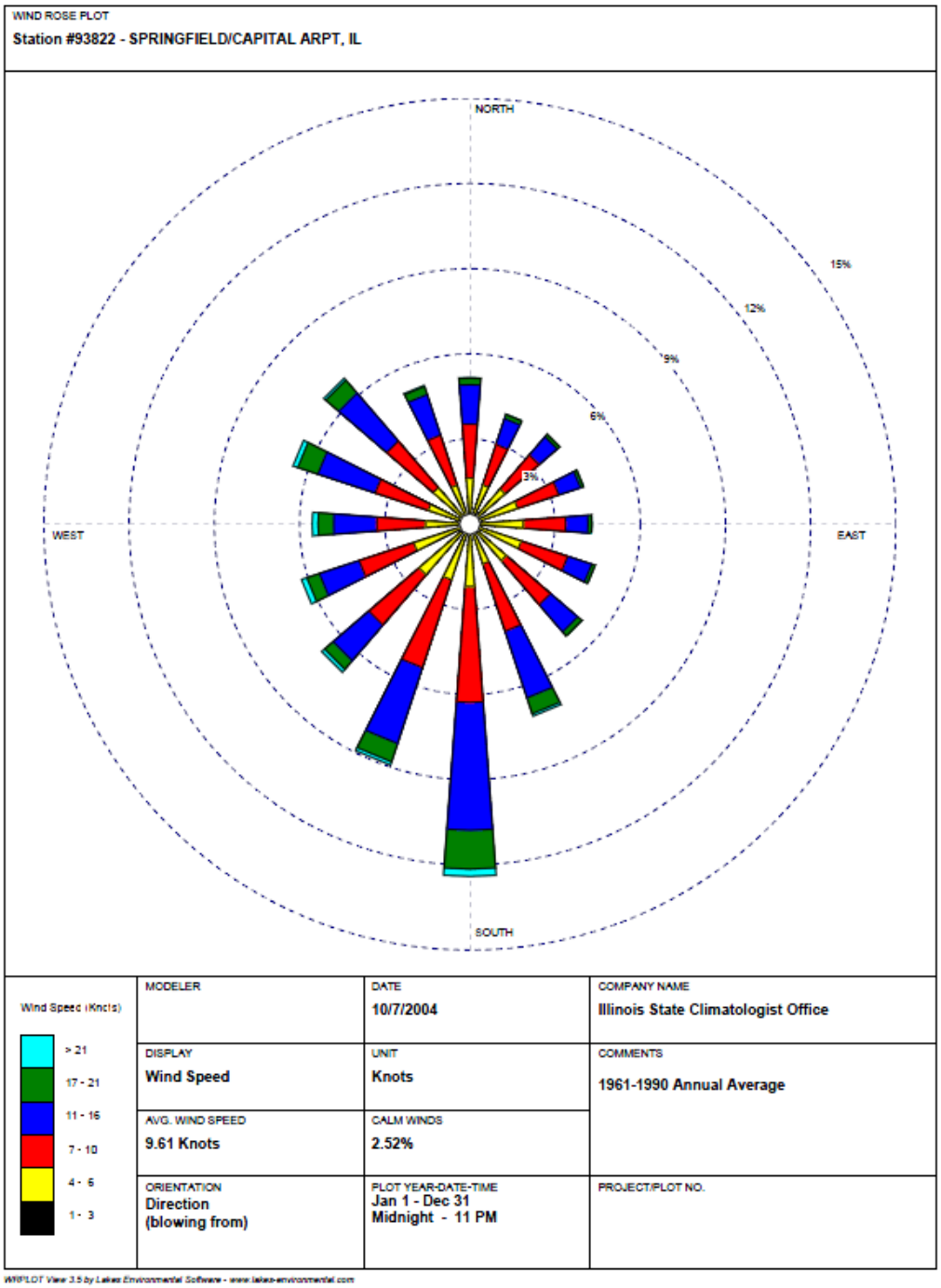

Figure 6. Average yearly wind directions and speed in Springfield, IL.

7. Modeling Approach

For this work, the commercial CFD code developed by Fluidyn, France (http://www.fluidyn.com/fluidyn/) called PANACHE/PANEPR has been used for modeling the transient formation, transport, and dispersion of CO_2 plumes following a hypothetical leak within the built environment of the plant. The CFD model was coupled with the pipe-decompression model (Pipe model) of Picard and Bishnoi (1988), which uses sophisticated equations of state and a fluid dynamic model to simulate the flow rate from a high-pressure pipeline as a function of time. This coupling was pursued in order to have precise estimates of the evolution of leakage rate with time at the pipeline rupture, that were used as source term in the dispersion model. Atmospheric dispersion simulations of various CO_2 pipeline leakage scenarios were carried out. Appendix B provides further description of the Pipe model. The methods used in PANACHE are described in Appendix C. In this section, we describe the use of PANACHE for modeling CO_2 pipeline leakage for the IBDP site.

7.1. Building the Model System

An interactive user interface built into PANACHE allows the convenient construction of the model system (e.g., placement of buildings, facilities, fields, etc.) using a map of the site as a background image. This model system is shown in Figure 7 in two-dimensions with the familiar overhead photo as background to orient the reader.

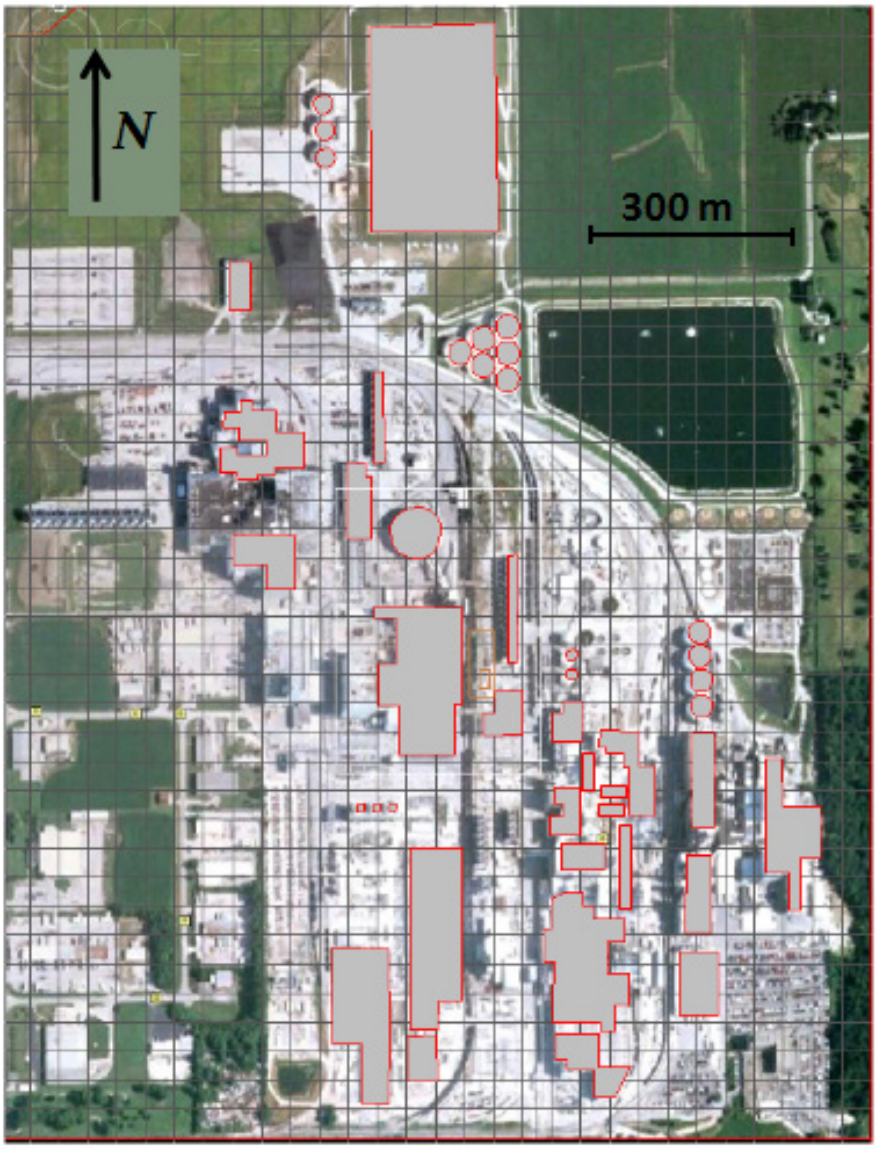

Figure 7. ADM's built environment as implemented in PANACHE. The gray shapes with red-borders are three-dimensional buildings and other flow obstacles considered by the model.

The third dimension of the buildings is shown in Figure 8. The two white-line-bordered polygons in the middle of the image, between the buildings, are domains where the mesh has been locally refined in order to better account for the jet-release from the leakage point. In fact, to model a high-speed flow, the code needs a relatively higher resolution internal mesh (large number of control volumes, CVs) to solve the Navier-Stokes equations and equations for turbulence generation/dissipation (see Appendix B) in proximity of the leak.

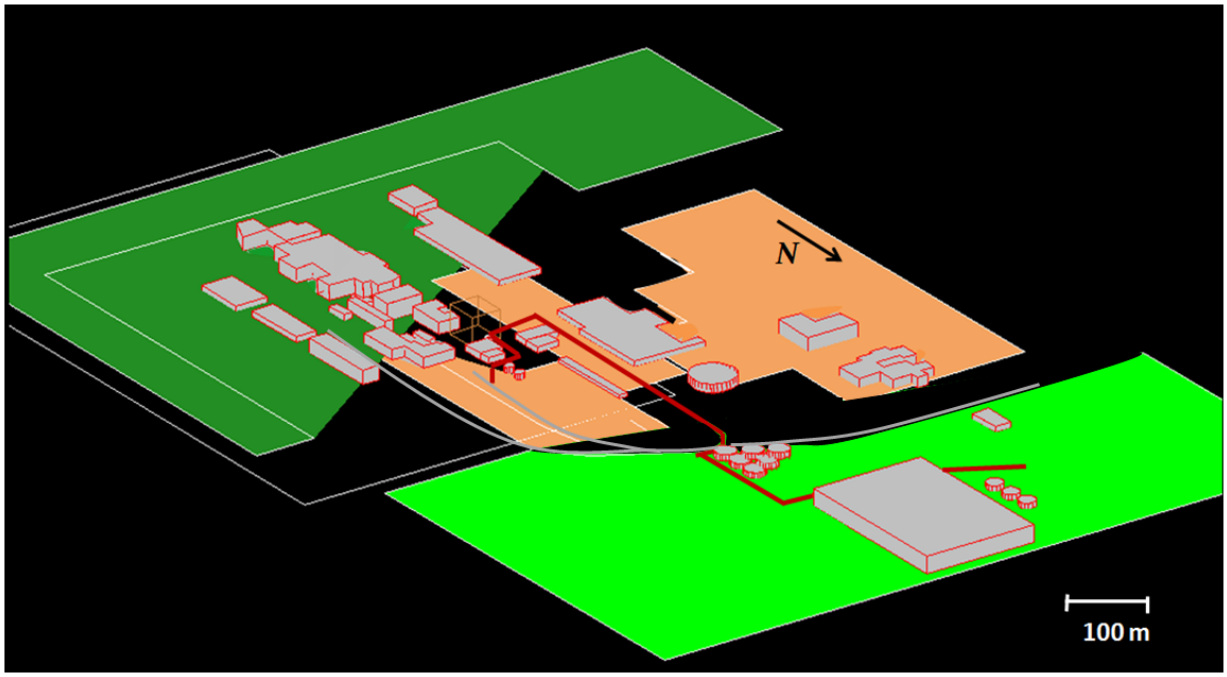

Figure 8. Oblique view of the ADM plant with major buildings as implemented in the model. The orange background represents a surface with roughness corresponding to an urban environment with buildings of height 5 m, the green color represents grassy field, and the dark green is forest. Some of the ground surface (black in the figure) was left without a specific roughness for better resolution when considering plumes of different gas concentrations. The dark red line is the pipeline.

Figures 6, 7, and 8 give a clear idea of the relative distances between modeled buildings. The space not occupied by the major buildings is filled at the ADM site by a variety of minor obstacles (e.g., smaller buildings, trucks, trains, pipelines, and facilities for loading and unloading grain). These smaller objects are accounted for in the model by specifying a surface roughness corresponding to an urban area (the orange region in Figure 8) with a characteristic average height of buildings (in this case 5 m). This specification is then converted by the model into a surface roughness parameter which is equal to one tenth of the average building height (in this case a surface roughness of 0.5 m).

7.2. Wind Field

Figure 9 shows the wind vectors for Scenarios 3 and 2 over areas considered in the atmospheric dispersion model after 100 s with between 200,000 and 400,000 cells (or CV's), each 0.1 seconds, for wind from weak to medium strength (1, 4, and 8 m/s)[2].

[2] In each trial simulated, the beginning of the release happens 400 s after the start of the simulation, to give PANACHE enough cycles to resolve the wind field consistently with the simulation location.

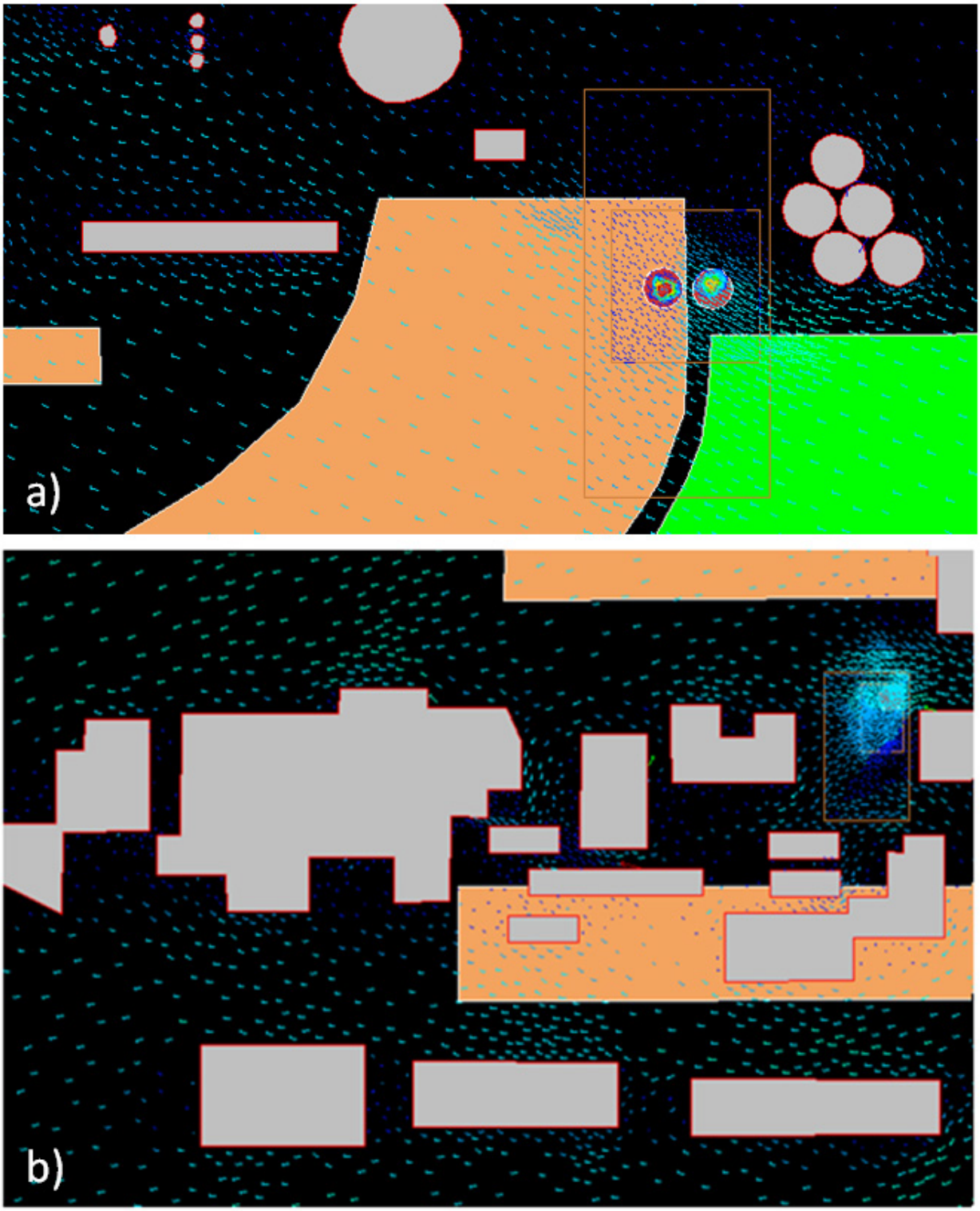

Figure 9. Wind fields before the beginning of the jet release for Scenarios 3 (a) and 2 (b) (see below). Note (Figure 9a) that the southeastern-most tank has been left out because it would have crossed the boundary of the nested domain, greatly affecting the creation of the mesh.

Figure 10 shows the wind fields (at the same locations as shown in Figure 9) 15 s after the beginning of the CO_2 leak, which is directed horizontally. It can be seen how the wind field is strongly modified by the high-speed expanding gas flow. Vectors in Figure 10 are strongly scaled (reduced in size), to accommodate the large velocities near the high-pressure pipeline rupture. Vectors representing 100 m/s flow velocity, set the upper limit in length (with respect to the initial average wind of 4 m/s).

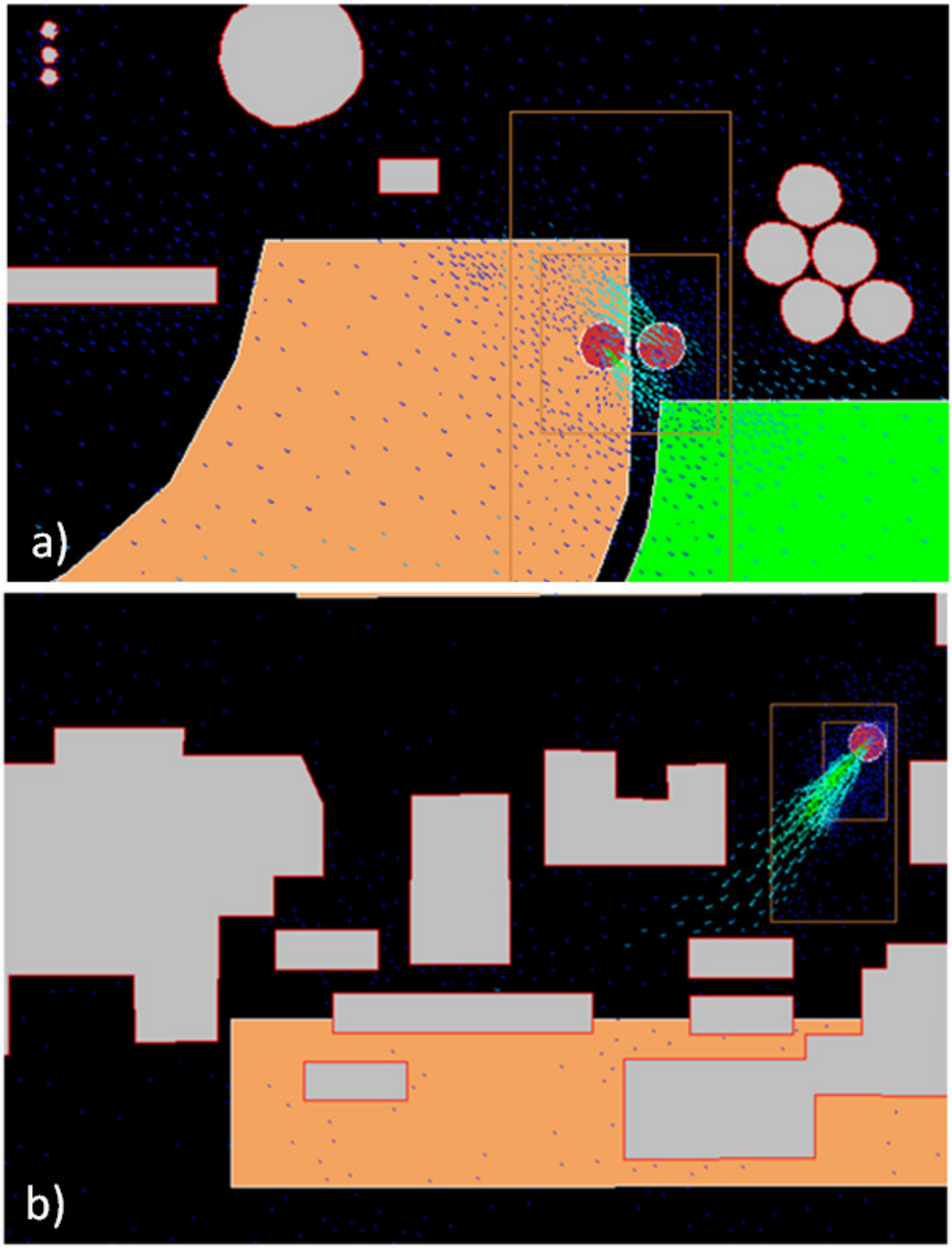

Figure 10. Wind velocity vectors 15 s after the start of the CO_2 release for Scenarios 3 (a) and 2 (b). The high-speed of the CO_2 leak prevents display of the natural wind around buildings when consistent scaling of wind velocity vectors is used.

8. Pipeline Failure Scenarios

8.1. Leakage Locations

Leakage locations in this study are assumed to be at places along the pipeline route where accidents, such as vehicles running into the pipe, are assumed to be most likely to occur. Figure 11 represents the route of the railway for grain delivery movement within the plant (green lines). Sites near loading and unloading locations are assumed to be the busiest environments during working hours in terms of vehicles and presence of ADM personnel.

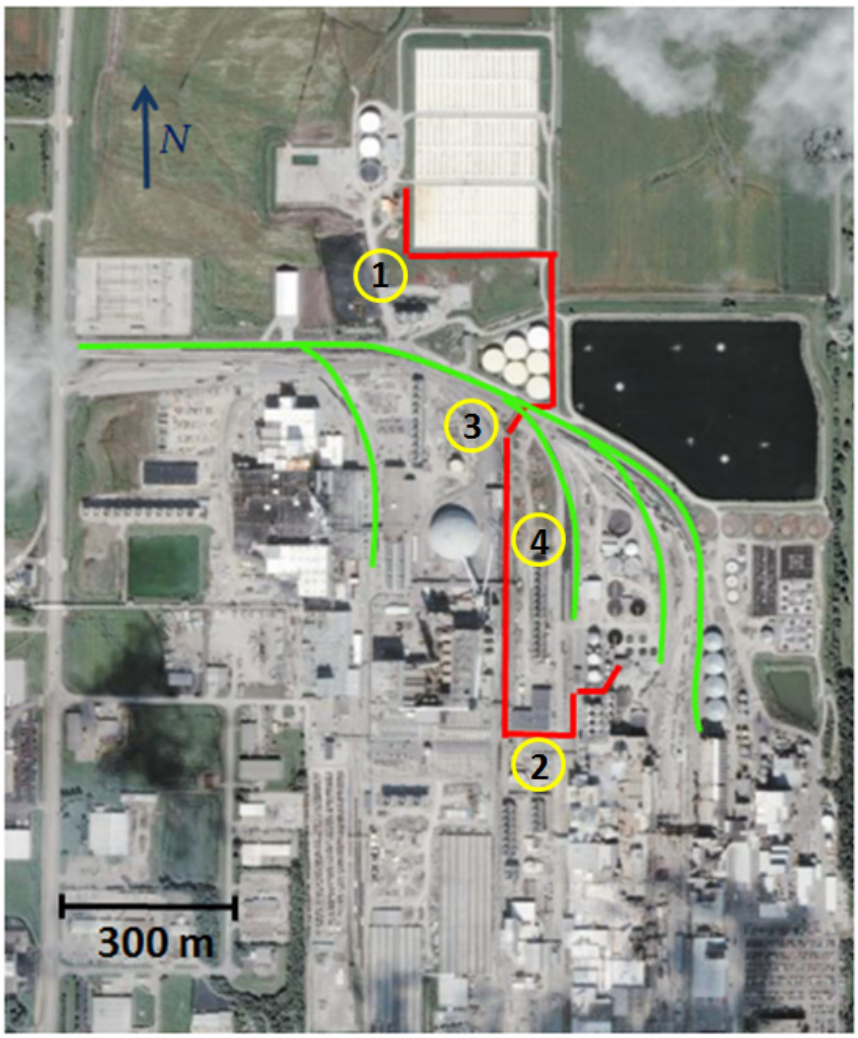

Figure 11. Route of the pipeline (red line) from the capture/compression facility (south) to the injection well (north). In green are displayed the railway lines within the plant.

CO_2 leakage scenarios from the pipeline are modeled as occurring at four locations as shown by the numbers circled in yellow on Figure 11. The locations are: (1) near the injection well; (2) near the capture/compressor facility, and (3, 4) along the pipeline route (Module 4 in Table 1), and specifically over the railway line and along the straight line of the pipe for over 500 m, before crossing the railway (Figure 11). Clearly accidents may occur at any location along the pipeline. Our choices were mainly based on the need for modeling the atmospheric dispersion of the gas in areas where it seemed most likely that accidents leading to pipeline leakage could occur.

8.2. Source Strength Evolution: Pipe Decompression Model

Usually, in order to determine the potential consequences from an accidental leak from a high-pressure gas transportation system, various failure scenarios will need to be considered, release scenarios determined, and release and dispersion modeling carried out. Hazard identification techniques and information from known incidents should be used to identify possible events for additional detailed analysis (Gale and Davison, 2004). Classical hazard analysis of chemical processes would aim to cover the whole range of hazardous events to obtain a model for the total risk from the process being considered, whereas, following the Precautionary Principle, studies to determine the most severe event need only model the consequences of the largest failure cases in the worst environmental condition (EI, 2010). In this study we have evaluated the consequences of maximum events during transport of CO_2 gas. Hence, our simulations all represent full-bore failures of the HP system.

Methodologies used in risk assessments and hazard analyses of gas transportation for evaluating emission rates from catastrophic leakage scenarios account for the strongly time-varying gas

leakage flow rate by feeding the dispersion model with a single time-averaged release rate source term. This method was used within the main studies dealing with safety of natural gas transportation and, recently, of CO_2 - e.g. (EI, 2010; Vendrig et al., 2003). This is a reasonable approximation of the real process if the decompression is rapid. Release cloud geometries can be depicted as time-averages, but the continuous process of atmospheric dispersion of a gas must be followed in time or else the consequences implied become overestimated. To improve the constant-release approximation, we have modeled the gas release rate using the Pipe model of Picard and Bishnoi (1988) as source term for the atmospheric dispersion modeled with PANACHE. The Pipe model uses sophisticated equations of state and a fluid dynamic model to simulate the flow rate from a high-pressure pipeline as a function of time.

As in every atmospheric dispersion model, the source term is the key input for the transport and dispersion processes. These are basically: emission rate (kg/s), duration (s), orientation in space of the leak (degrees on the XY and XZ planes), and velocity of the gas (m/s).

In the simulations run for this study, these values have been taken from two runs of the Pipe model, accounting for the total decompression of 500 m and 1,000 m long pipelines after their complete failure (i.e., a full-bore leak). Tables 3A and 3B display the characteristics of the two pipeline segments considered, the fluid carried (supercritical CO_2) and its flow through the pipe. An important parameter, used to evaluate the duration of the releases in the simulation, is the initial amount of gas in the pipe. Obviously, the 500 m pipe contains half of the initial substance relative to the 1,000 m pipe. To be conservative, we have modeled the source with a total amount of CO_2 available for dispersion of 1,000 kg higher than the real value, for both source terms.

Tables 3A and 3B. Transportation system characteristics and leakage details. Highlighted are the lengths and masses of the pipes considered.

Pipe Details	**A**
Length of the Pipe (m)	1000
OD of the Pipe (m)	0.1683
Pipe Thickness (m)	0.011
ID of the Pipe (m)	0.1463
Pipe Roughness (m)	4.60E-05
Fluid Details	
Initial Pressure of Fluid (kPa)	10101.325
Initial Temperature of Fluid (°C)	15
Density of Fluid (kg/m^3)	830.36
Viscosity of Fluid (mPa.s)	0.0783
Speed of Sound in Fluid (m/s)	427.65
Cp/Cv Ratio	3.13744
Flow Details	
Area of Flow (m^2)	0.016810419
Inertial Correction Factor	1
Initial Mass Flow Rate (kg/s)	5969.496693
Reynolds Number	663501251.6
Moody Friction Factor	1.51E-02
BA factor	1.55E+00
Beta	61.43927881
Initial Mass in the Pipeline (kg)	13958.72413
Alpha	0.038059397

Pipe Details	**B**
Length of the Pipe (m)	500
OD of the Pipe (m)	0.1683
Pipe Thickness (m)	0.011
ID of the Pipe (m)	0.1463
Pipe Roughness (m)	4.60E-05
Fluid Details	
Initial Pressure of Fluid (kPa)	10101.325
Initial Temperature of Fluid (°C)	15
Density of Fluid (kg/m^3)	830.36
Viscosity of Fluid (mPa.s)	0.0783
Speed of Sound in Fluid (m/s)	427.65
Cp/Cv Ratio	3.13744
Flow Details	
Area of Flow (m^2)	0.016810419
Inertial Correction Factor	1
Initial Mass Flow Rate (kg/s)	5969.496693
Reynolds Number	663501251.6
Moody Friction Factor	1.51E-02
BA factor	1.55E+00
Beta	21.74242197
Initial Mass in the Pipeline (kg)	6979.362063
Alpha	0.053773721

The ability to make realistic predictions of the temporal evolution of the flow rate out of the pipe greatly improves the reliability of risk assessment for human asphyxiation, because the size of the plume is a direct function of the amount of gas available for dispersion (i.e., the leakage flow rate).

As stated above, the Pipe model was used for considering two different releases: (a) a full-bore release at one end of the ~1 km pipe (Source A in the results presentation section); and (b) a full-bore failure in the middle of the pipeline (defined as Source B). Figure 12 presents a diagram

describing the decompression history in terms of leaking rate strength over time for the first process considered (single decompression of a 1 km pipe).

The graphs in Figures 12 and 13 display the characteristic values for the releases considered in the scenarios. Note how transient release rates calculated by the Pipe model were discretized into five or six constant sources within PANACHE, with an increasing velocity of the leaking gas with time. The enhancement of the speed of the gas as it leaks out of the pipe with time is due to the non-linear function representing the density of the substance against pressure. Basically, as the pipe decompresses, the density of CO_2 decreases making the velocity increase for a given mass flow.

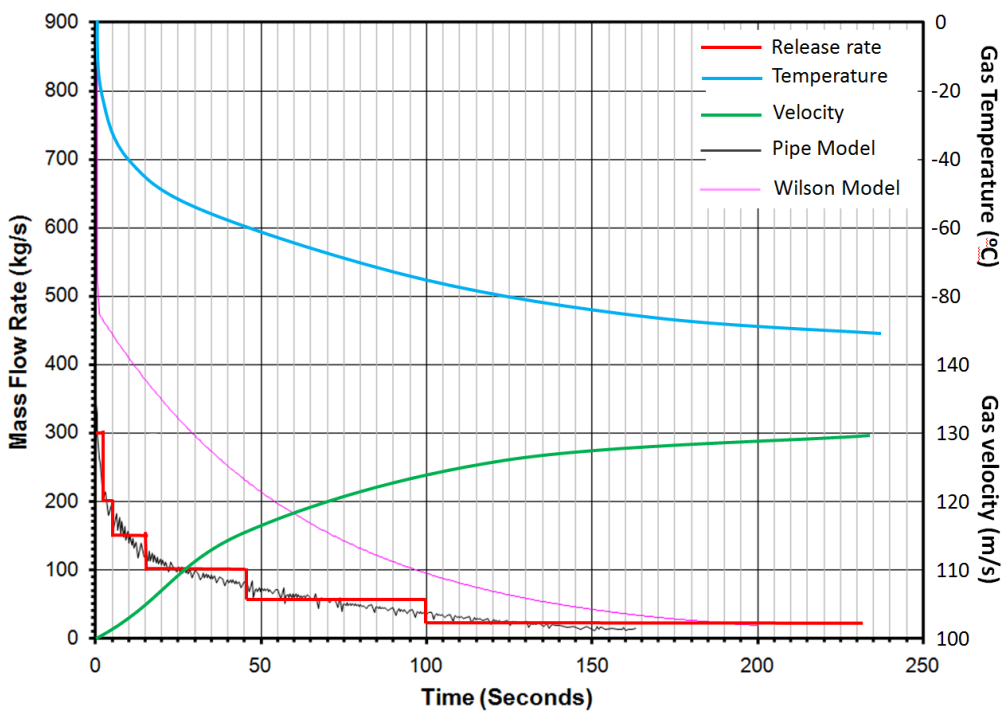

Figure 12. Modeling of full-bore leakage-rate evolution in time. The black line represents the release rate as modeled by the Pipe model for the 1 km scenario (Source A). Flow rates have been discretized into six steps of constant release for input into PANACHE (red line). The violet line is the release calculated with the Wilson model (not used here); the green line represents the velocity of the gas exiting through the broken end of the pipe with time and the blue line represents the temperature of the leaking gas as it develops with in-pipe pressure/time.

The scenario considered represents a decompression occurring after a pipeline failure near the start or the end of the pipeline and consists of a time varying singular transient release. For modeling gas dispersion after the occurrence of a failure near the middle of the pipe, the simultaneous decompression of two pipes of 500 m length is considered. We assume (Simulations 3 and 4) that the two broken ends of the pipe would release the amount contained in the two 500 m segments created after complete failure contemporaneously, from two very near point sources, with opposite emission directions. The description of the development of the source strength for this scenario is displayed in Figure 13 (for one of the broken-off pipelines).

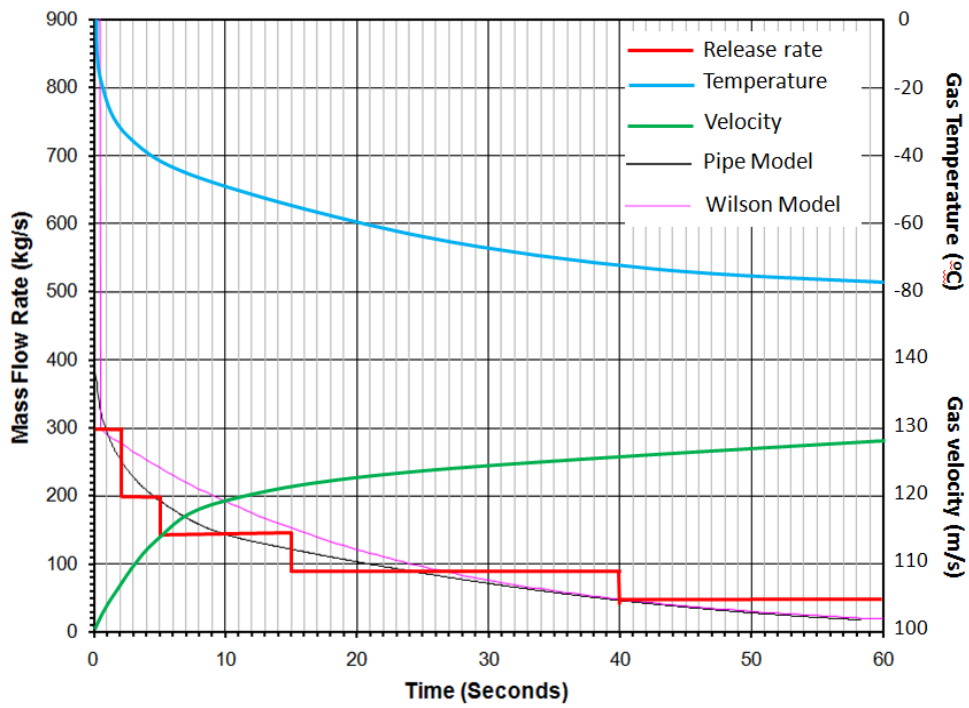

Figure 13. Model full-bore release rates and exit velocity as a function of time. The black line represents the release rate modeled by the Pipe model, for the 500 m scenario. Leakage rates have been discretized into five steps of constant release within PANACHE (red line). The violet line is the release calculated with the Wilson model (not used here); the green line represents the velocity of the gas exiting through the broken end of the pipe and the blue line represents the temperature of the leaking gas as it develops with in-pipe pressure/time.

From Figures 12 and 13, it can be seen how, for the two release-events considered, the instantaneous leakage rates at diverse times after beginning, are comparable. It is well known in fact that for high-pressure pipeline leakage events, the change in length of the pipe does not have much effect on the release rates at the beginning of the event, but rather modifies the overall duration of the release (Jo and Ahn, 2002; Yuhua et al., 2002). For the two scenarios of Figures 12 and 13, the main difference is in the duration of the leak. The 500 m source in fact takes about 100 s for discharging all its content, while the longer pipe needs up to 300 s to release all the gas. In the results section, simulations 1 and 2 were run with Source A, while Simulations 3 and 4 were run with Source B. To account for an incomplete shut-off of CO_2 sources at either end of the pipe, in all of the simulations we have continued the CO_2 release with an arbitrary value of 10 m s^{-1} leakage velocity for an additional 200 seconds beyond the time when the release becomes dominated by the CO_2 supply to the pipe as opposed to pipe decompression.

9. Atmospheric Dispersion of CO_2 Within the Plant and Assessment of Risks

9.1. Introduction

In this section we present simulation results of atmospheric dispersion of CO_2 arising from leakage scenarios involving the pipeline system built within the ADM ethanol plant for transporting CO_2 from the capture facility to the injection well, during its proposed three-year period of operation. Four failure scenarios at different locations along the pipeline route have been considered. Given the importance of the pipeline route for both creating likelihood of rupture and hazard of CO_2, we describe the pipeline route before presenting results for the four failure scenarios.

9.2. Pipeline route

Although pipeline failure could occur at any point along the length of the pipeline, the path of the existing above-ground pipe is analyzed from the capture site to the injection well in order to highlight key regions where we believe the risk (likelihood multiplied by potential consequences) of pipeline leakage is higher than along other lengths of the pipe and which therefore influenced our choice for the locations of failure scenarios. We save for a later section a discussion of mitigation recommendations and strategies within the plant environment. In Figure 14, we indicate the locations of the four scenarios. The green circle shows the location where the pipeline is elevated to pass over the railroad.

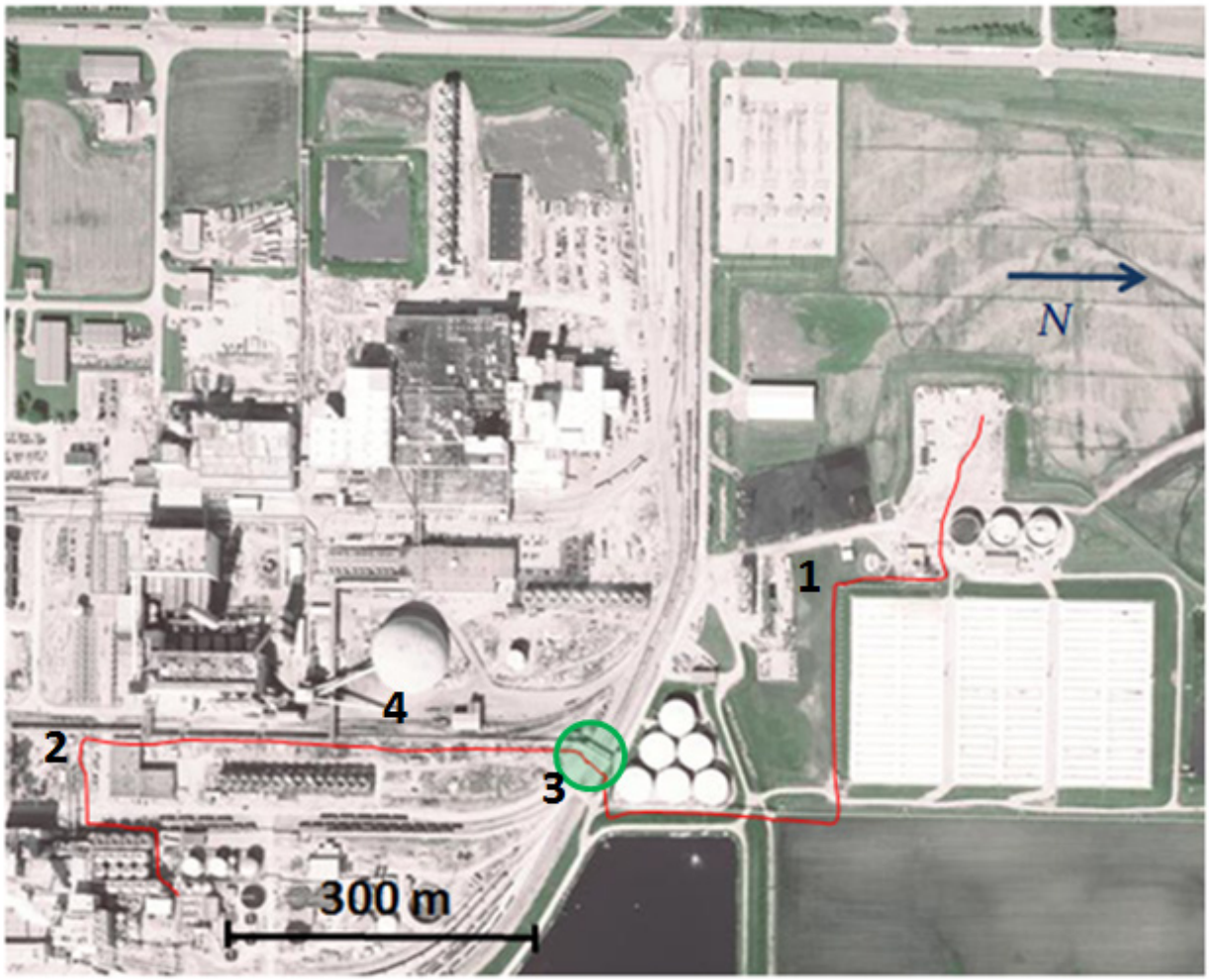

Figure 14. Overhead view of the plant with leakage locations of Scenarios 1-4 indicated. The pipeline is elevated several meters above ground to pass over the railroad tracks at the location of the green circle (Scenario 3).

Figure 15 shows an image representing the capture station (beginning of the transportation system) with technical elements identified. As shown in the figure, after leaving the compressor, soon after separation from other waste gases within the capture plant (Figure 15), the pipeline follows other pipelines above-ground at about the height of a person, before subsequently crossing, via overhead sections, vehicular roads and other passages for people and goods.

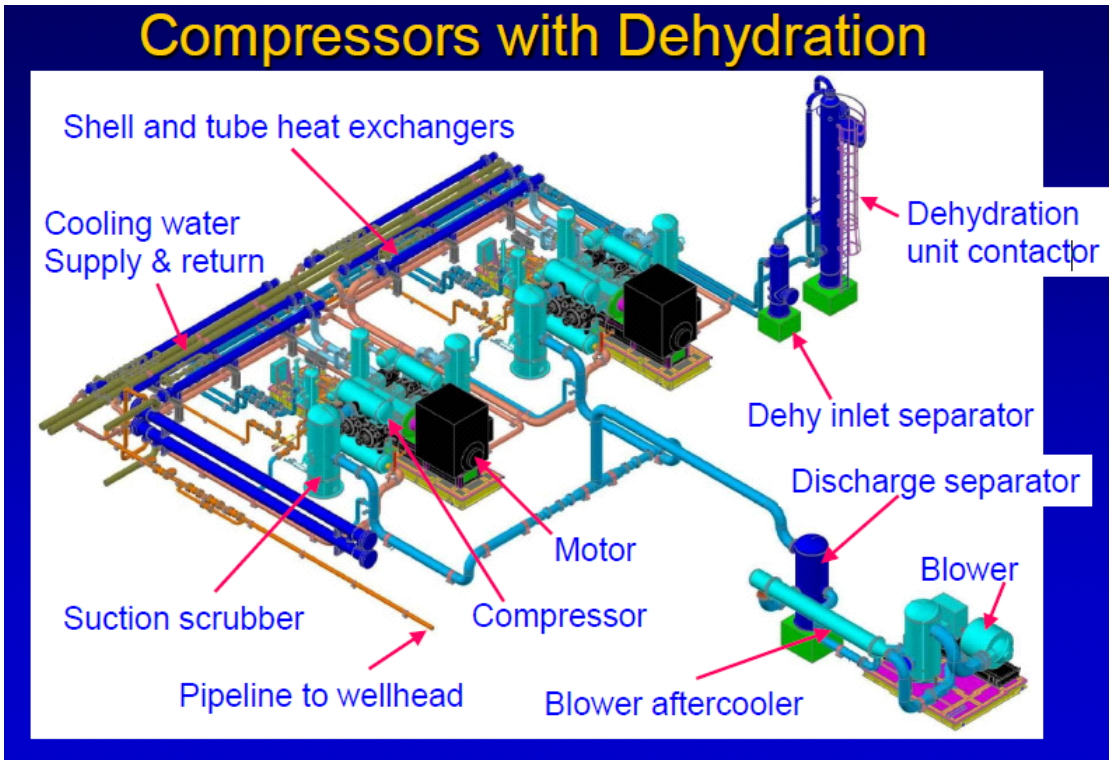

Figure 15. The capture and compression station at the ADM plant.

The pipeline bends several times at 90 degrees and makes an overhead crossing of the main vehicular artery serving the heart of the plant, which we assume is relatively busy with vehicular traffic. Following this, the pipeline follows a straight line north for about 500 m until it bends upward an additional 2 m to reach a eight of 4 m in order to cross the railroad tracks show in Figure 14 by the green circle. We believe this elevated section of the pipeline is the most vulnerable part of the pipe, due to the possibility of a train hitting the pipeline with objects it may be carrying. As discussed previously, even a rupture that is initially small could develop into a propagating fracture that would quickly develop into a full-bore leak[3].

[3] Propagating fractures usually develop along the length of a failing high-pressure pipe, they would then result into a linear leaking source, rather than into a full-bore, point source. The former would present a much lower hazard.

After crossing the railroad, the pipeline enters an area presumably less frequented by plant personnel. Although protected along the route because it is located alongside storage facilities, the pipeline crosses wider areas where the presence of moving vehicles is possible, with associated possibility of accidents that could involve the pipeline itself.

9.3. Leakage and Dispersion

We have modeled four scenarios chosen to account for the different local environments crossed by the pipeline. As delineated above, two different source terms are considered in the four simulations, one for leaks near the compressor station or the injection well (i.e., end of pipe) and one for leaks occurring near the middle of the pipeline route. The two classes of source terms are needed due to the fact that, while a full-bore leak at one end of the pipe could be seen as a single source releasing all of the pipeline's CO_2 content (the other part of the cut pipe containing a relatively small amount of gas), a failure near the middle of the pipeline needs to be treated as a double source. A double source emits the same total amount of gas but it does so from two detached points, therefore at a higher flow rate.

In the two release simulations that considered the double-source scenario (Scenarios 3 and 4), the sources were modeled as leaking points releasing their content in opposite directions as if the pipe were severed and the two ends offset by at least one pipe diameter.

Figure 16 shows the areas of the plant where the main CO_2 dispersion-cloud develops for each of the four pipe-rupture points.

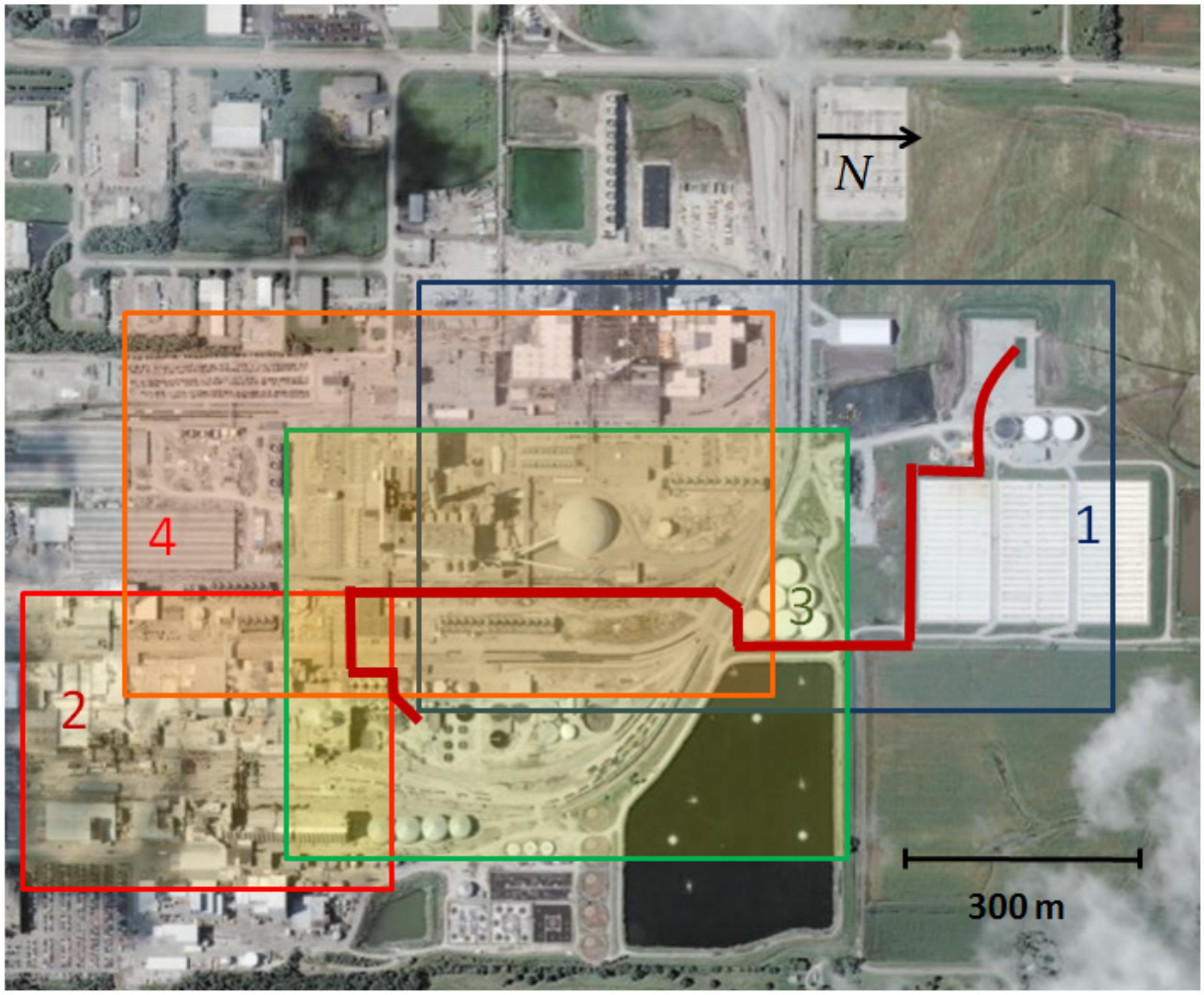

Figure 16. Pipeline route (thick dark red line) and areas where CO_2 dispersion is considered in the following simulations.

In the following pages, the physical process of CO_2 atmospheric dispersion is described with the help of sequential shots displaying on the horizontal plane the simulated development of the CO_2 concentration field for given release rates, flow velocity, leak direction, atmospheric conditions, and building distribution.

In order to account for major buildings and other minor obstacles, the wind field was resolved during the first 400 s of the simulation (the release starts formally at t = 400 s). However, throughout the presentation and discussion of results (figures and text, below) t = 0 is considered

to be the time of the start of CO_2 release. The first results shown for each of the four scenarios contains a plot of the wind velocity field after 380 s from the start of the simulation (not of the release, which occurs at t = 400 s). The wind speed is described in the images with wind vectors of different lengths and colors (Figures 17, 19, 21 and 23), where reddish colors (right-hand side of the scale at the bottom of the images) represent the faster air/gas velocities encountered and colors near the blue end represent slower air/gas velocity. We also present an oblique aerial view of the plume concentrations at various times after the beginning of the release (Figures 17, 19, 21 and 23).

The description of a characteristic gas dispersion simulation in the ADM environment proceeds with the presentation of a sequence of figures showing the dispersing gas through concentration (ppm) contours in the horizontal (XY) plane (ground surface of plant) at different times after the start of the release. In the figures, concentrations of 40,000 ppm, 100,000 ppm and 250,000 ppm are shown in white, blue and red color, respectively. Concentrations of 10,000 ppm and below are represented as color contours of decreasing concentration lying on the XY plane (ground surface), with colors ranging from red (10,000 ppm) to blue (380 ppm = atmospheric concentration). The range of concentrations below 10,000 ppm does not present an acute health hazard but serves to locate the dispersing plume.

9.4. Scenario 1

The first Scenario for CO_2 dispersion models a full-bore leak near the end of the pipeline route, in the proximity of the injection well. Wind comes from NNE and has an average speed of 4 m/s (9 mph), at a height of 10 m (33 ft). The release rate considered in this simulation corresponds to

Source A (Figure 12). The wind field of Figure 17a corresponds to a time just before the start of the release, while the CO_2 concentration field in Figure 17b is after 90 s of CO_2 release.

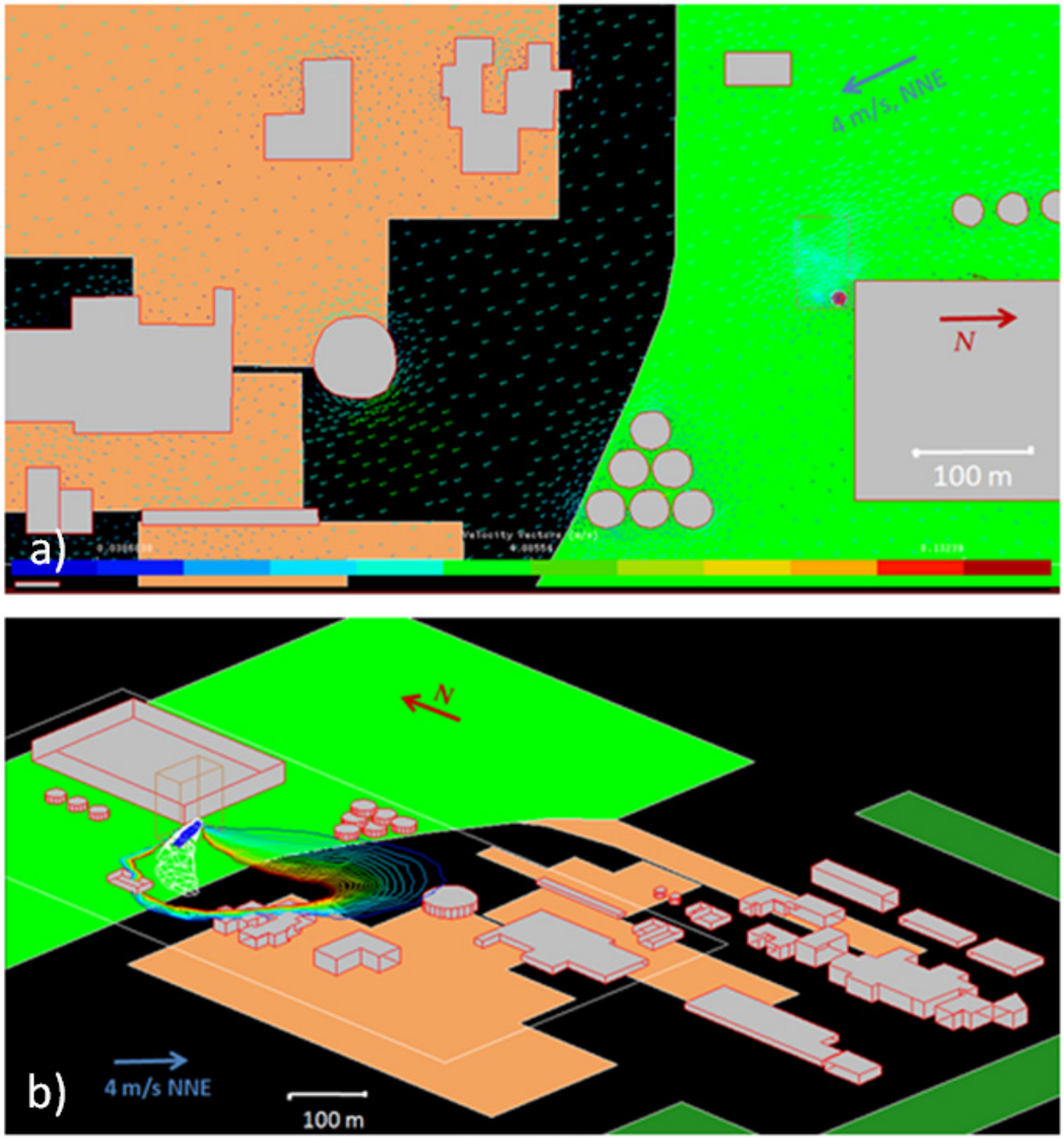

Figure 17. Simulation results for Scenario 1. (a) Wind velocity field in the area of dispersion as modified by the presence of buildings. (b) Oblique view of the model plant showing results at t = 90 s of the 100,000 ppm contour surface (blue region near leakage source), 40,000 ppm isosurface (white surface), and 10,000 ppm and lower color contours on the ground surface. The red surface representing 250,000 ppm is very small and not visible in this figure.

Figure 18 shows the dynamic process of atmospheric dispersion of the dense gas in time. The time evolution of the concentration of 40,000 ppm contour can be observed by following the white contour in the sequence of images. Due to the direction of the moderately strong wind, perpendicular to the axis of the resulting jet flow, the plume remains narrow in width (about 40 m at its maximum), being elongated away from the source. It reaches a maximum down-stream length of 300 m at about t = 100 s, then decreases in dimension as it is being dispersed by the wind, and eventually disappears about 3 minutes after the start of the leak.

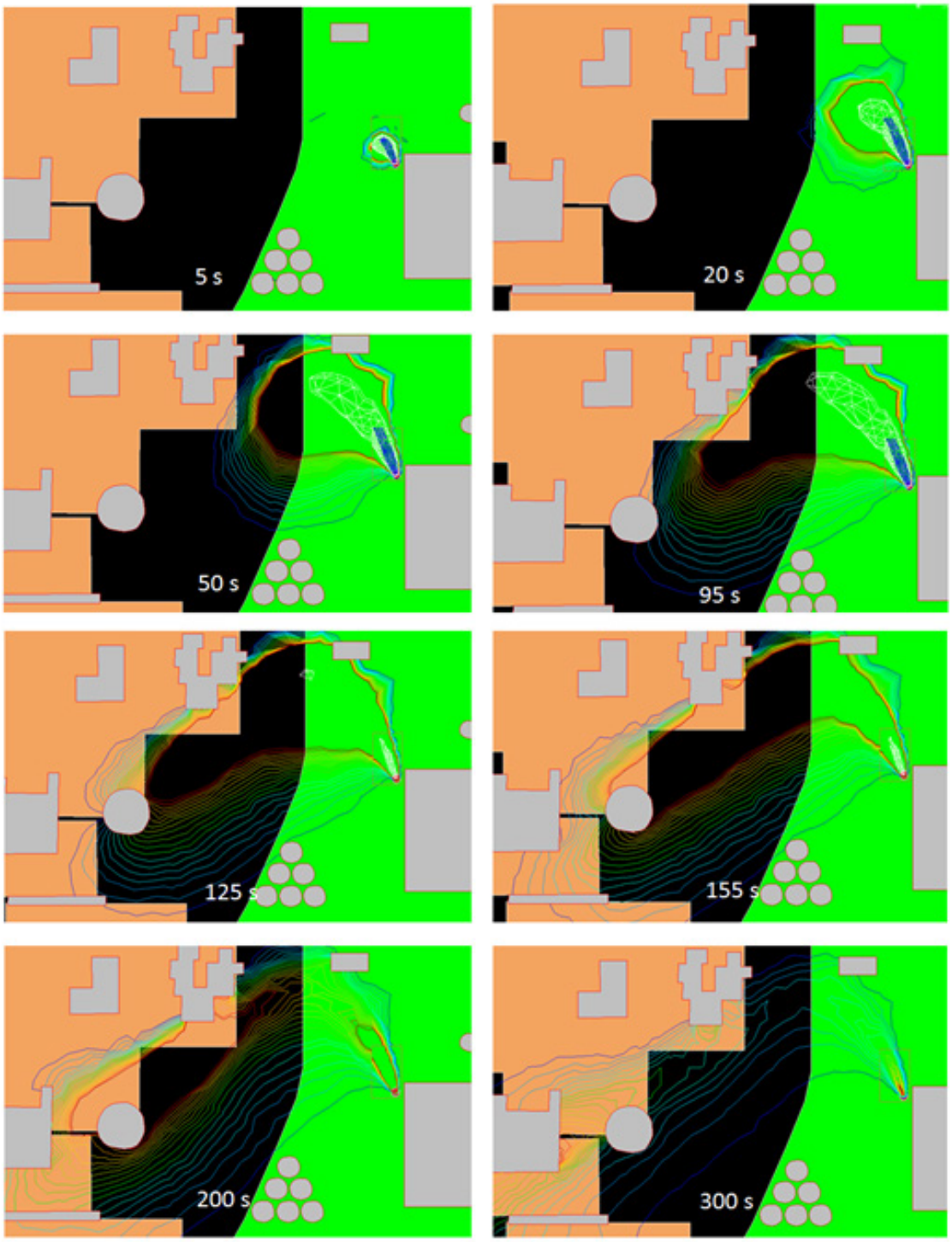

Figure 18. Simulation results showing the CO_2 isoconcentration lines (see text) at eight times following the start of the leak for Scenario 1.

As shown in Figure 18, the 100,000 ppm concentration isopleth (blue surface) follows the development of the 40,000 ppm isopleth at early times, but reaches its maximum size much earlier, at about t = 15 s. With the sequential constant release rate values considered for the description of the transient leak, this toxic plume keeps its maximum downstream length of 80 m for about 100 s and then disappears as the release rate decreases. The concentration of 250,000 ppm attains a steady maximum distance away from the source of < 5 m and cannnot be resolved in the images presented for this simulation.

9.5. Scenario 2

The second Scenario was chosen to assess the atmospheric hazard created after a complete failure of the system near the source of the captured gas. Basically, this simulation comprises a release of CO_2 near a densely built environment within the plant, in which offices and other locations that deserve particular attention are present. The direction of the release (coming from NNW), again of type Source A, has been chosen in order to depict a scenario of high risk: the jet-flow points toward a location characterized by potentially occupied indoor and outdoor working environments.

As with the previous Scenario 1, Figure 19 is composed of two figures. The first represents the characterization of the wind field, while the second image is an oblique view of the dispersion process, at t = 130 s. From this figure it can be noted how the 40,000 ppm concentration surface is pushed upward by the presence of the buildings.

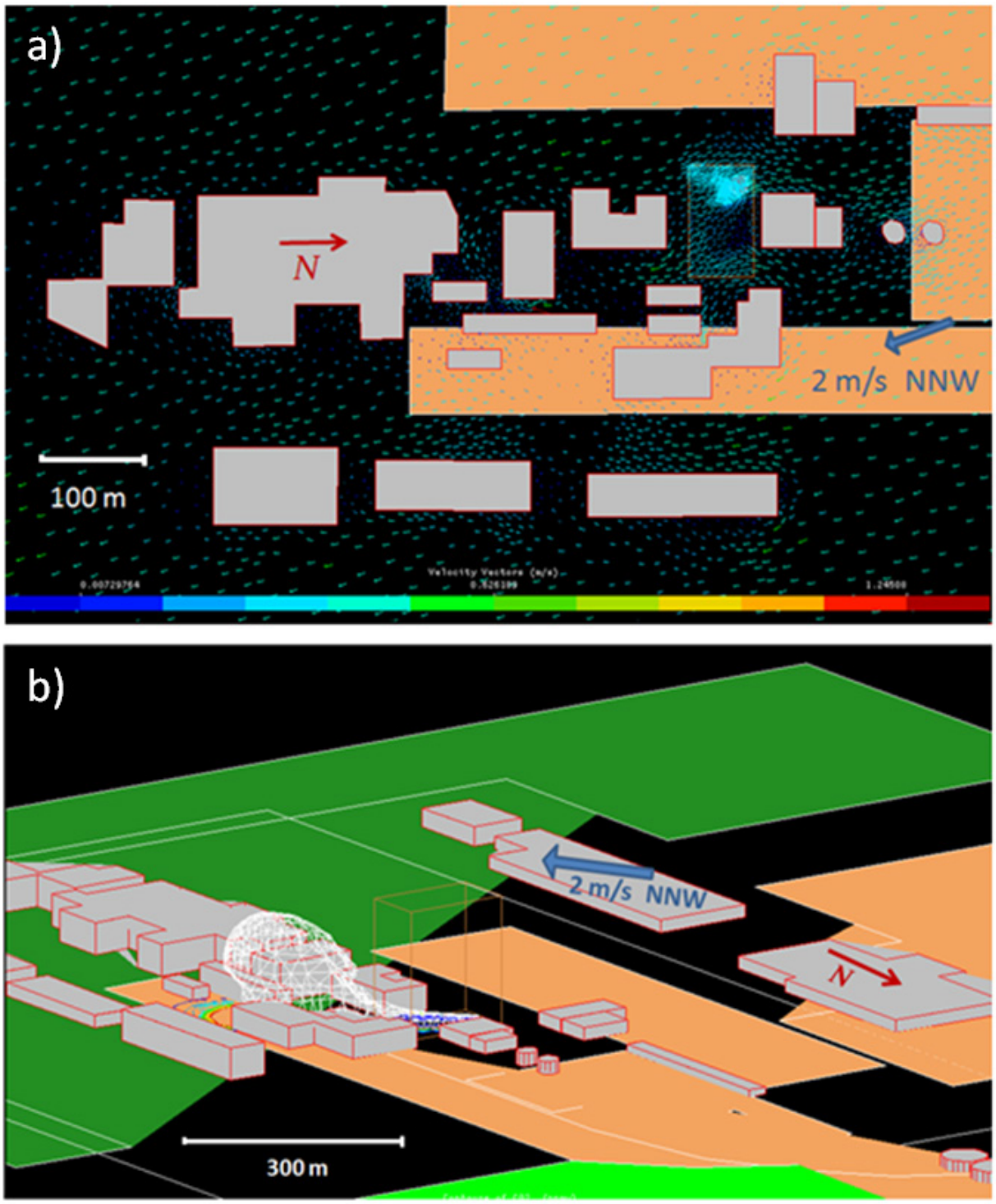

Figure 19. Simulation results for Scenario 2. (a) Wind velocity field in the area of dispersion as modified by the presence of buildings. (b) Oblique view of the model plant showing results at t = 130 s of the 100,000 ppm contour surface (blue region near leakage source), 40,000 ppm isosurface (white surface), and 10,000 ppm and lower color contours on the ground surface. The red surface representing 250,000 ppm is very small and not visible in this figure.

Figure 20 shows the evolution of the plume at six times after the start of the release. The 40,000 ppm isopleth (white surface) is strongly influenced by the built environment. It reaches its maximum size after about 3 minutes of continuous release and then dissipates slowly among the buildings. The 40,000 ppm isopleth is still present 15 minutes after the start of the release at some locations in this scenario. The 100,000 ppm isopleth develops within a volume not directly intersected by the buidings. It reaches a maximum downwstream length very soon, arriving to a distance of about 120 m away from the rupture. Because of the absence of strong turbulence, this concentration remains in place for over 3 minutes, subsequently dissipating among the buildings. It should be noted that, although this concentration does not seem to affect directly the built environment, slightly lower concentrations could intrude into a room through an open window or ventilation system and accumulate quickly within the indoor environment, posing a very high risk for people present. The concentration of 250,000 ppm can be seen in the images, reaching a maximum downstream value of almost 20 meters from the leaking source.

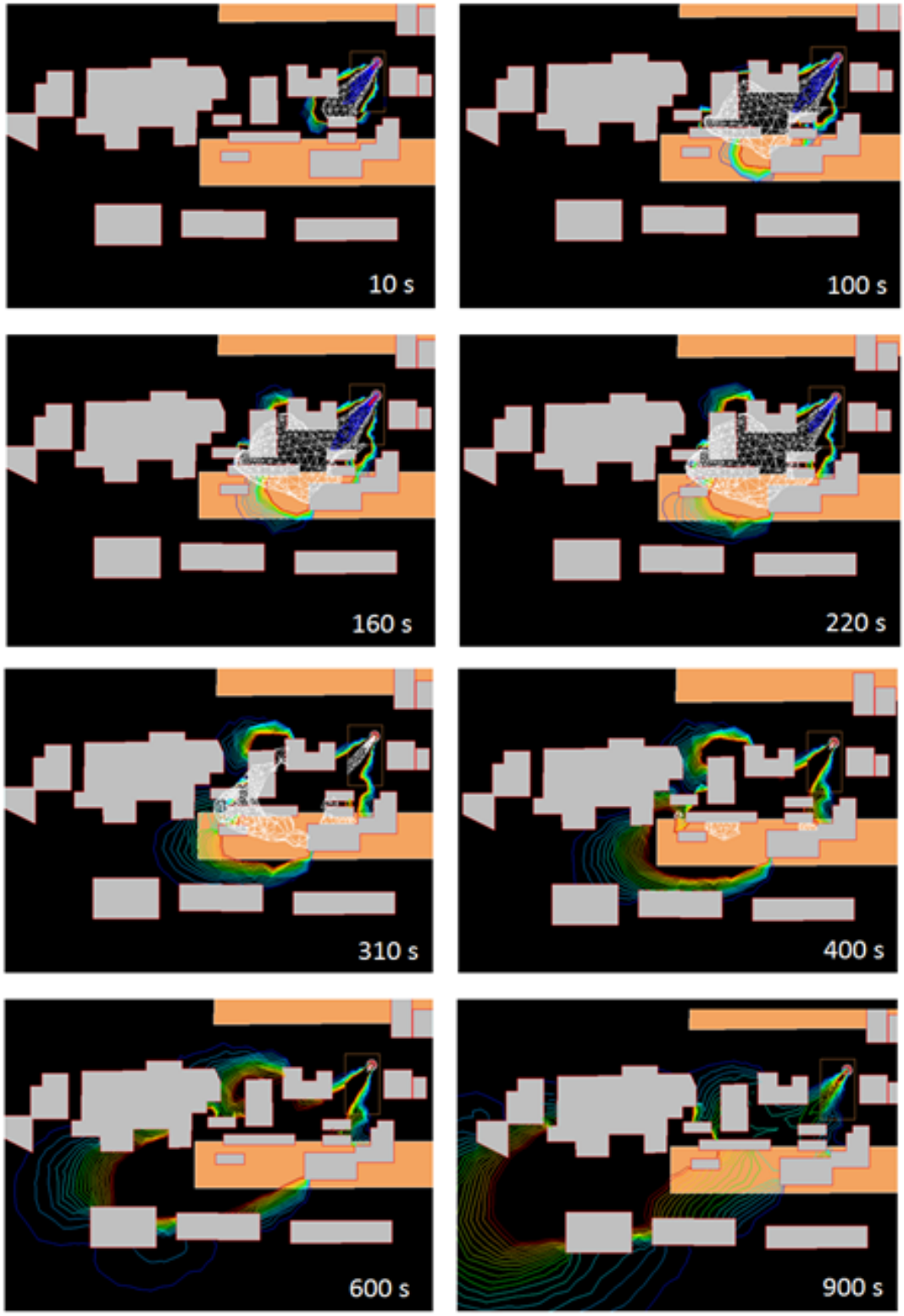

Figure 20. Simulation results showing the CO_2 concentration isopleths (see text) at eight times following the start of the leak for Scenario 2.

9.6. Scenario 3

This Scenario represents a double-source release caused by a complete failure of the transmission pipe near the middle of its length, more precisely, above the railway, at a height of 4 m. The simulation uses a Source B (Figure 13), meaning two contemporaneous point sources with the same release rate evolution with time, emitting CO_2 in the horizontal plane (as are all other releases considered in this study) and with opposite direction. The effects of the buildings on the strong wind are visually displayed in Figure 21, together with the oblique view of the dispersion process at time t = 190 s. The different relations of the oppositely-directed jet flows with respect to the wind vectors -- basically one release points windward and the other leeward -- can be seen in the figure as the relatively strong wind (8 m/s or 18 mph) influences the development of the resulting cloud.

Note that due to issues related to the difficulty of creating the mesh when buildings cross the boundary between two meshing domains, one of the cylindrical silos among the six present in proximity to the source, was omitted for this scenario.

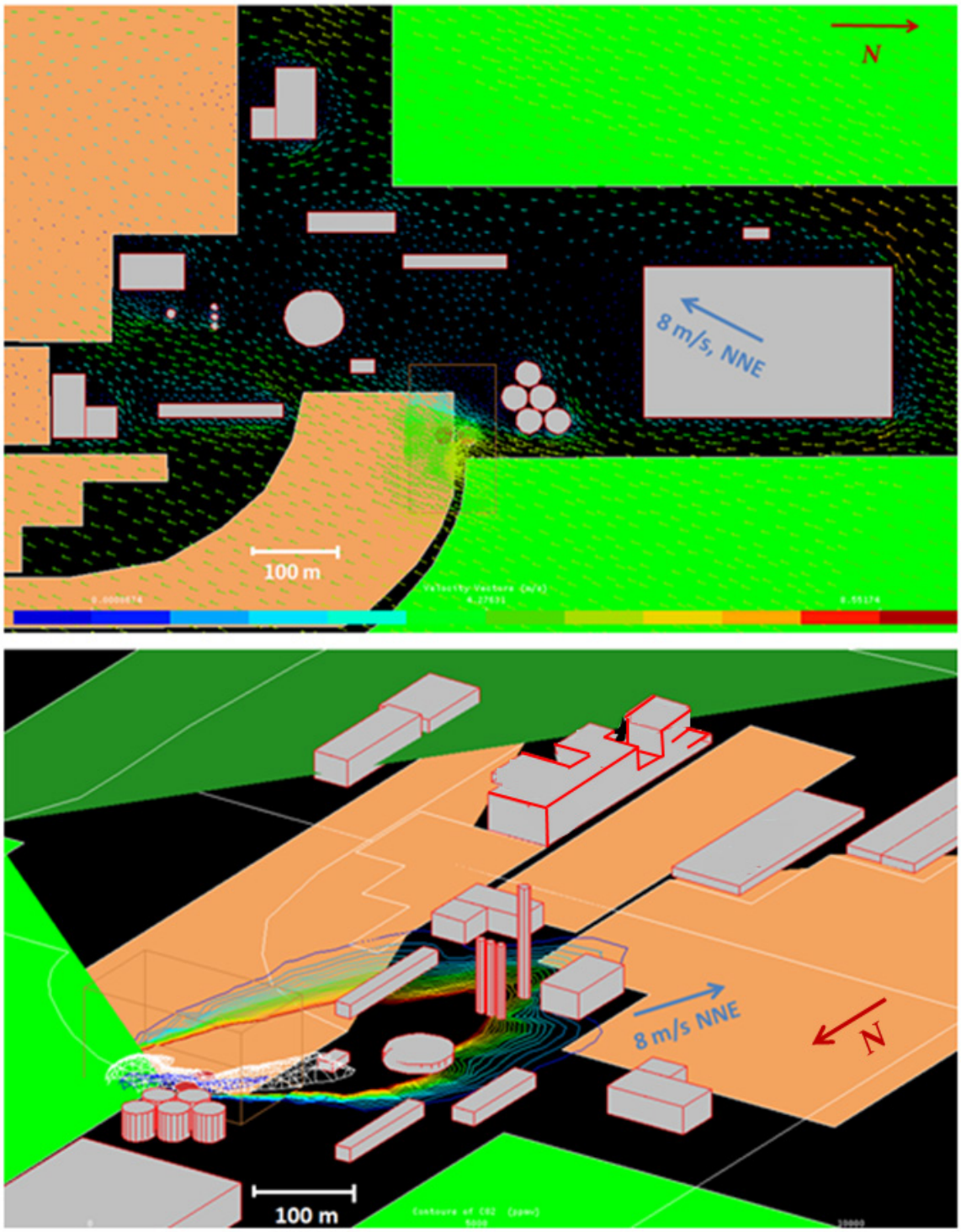

Figure 21. Simulation results for Scenario 3. (a) Wind velocity field in the area of dispersion as modified by the presence of buildings. (b) Oblique view of the model plant showing results at t = 190 s of the 100,000 ppm contour surface (blue region near leakage source), 40,000 ppm isosurface (white surface), and 10,000 ppm and lower color contours on the ground surface. The red surface representing 250,000 ppm is visible near the rupture point.

Figure 22 displays the time evolution of the concentration after the leakage event. It can be seen from the image how both the concentration of 100,000 and 40,000 ppm stabilize after approximately 30 s from the start of the leak. The upwind part of the release is clearly more influenced by the wind than the downwind side of the leak. In both release jets, the concentrations remain in place for longer than 5 minutes, then, after the release rate decreases, the strong wind (8 m s^{-1}) dissisipates the plumes. The 100,000 ppm concentration covers a relatively wide area, with the sum of the maximum downstream distances covered by the two opposite releases being larger than 150 m. This large plume width is aided by the fact that the horizontal release is placed at 4 m elevation above the railway. The choice to model a horizontal leak was dictated by the desire to simulate scenarios of high risk; in fact, horizontal releases produce larger plume areas. The upwind part of the 40,000 ppm isopleth is strongly affected by the oppositely-directed wind.

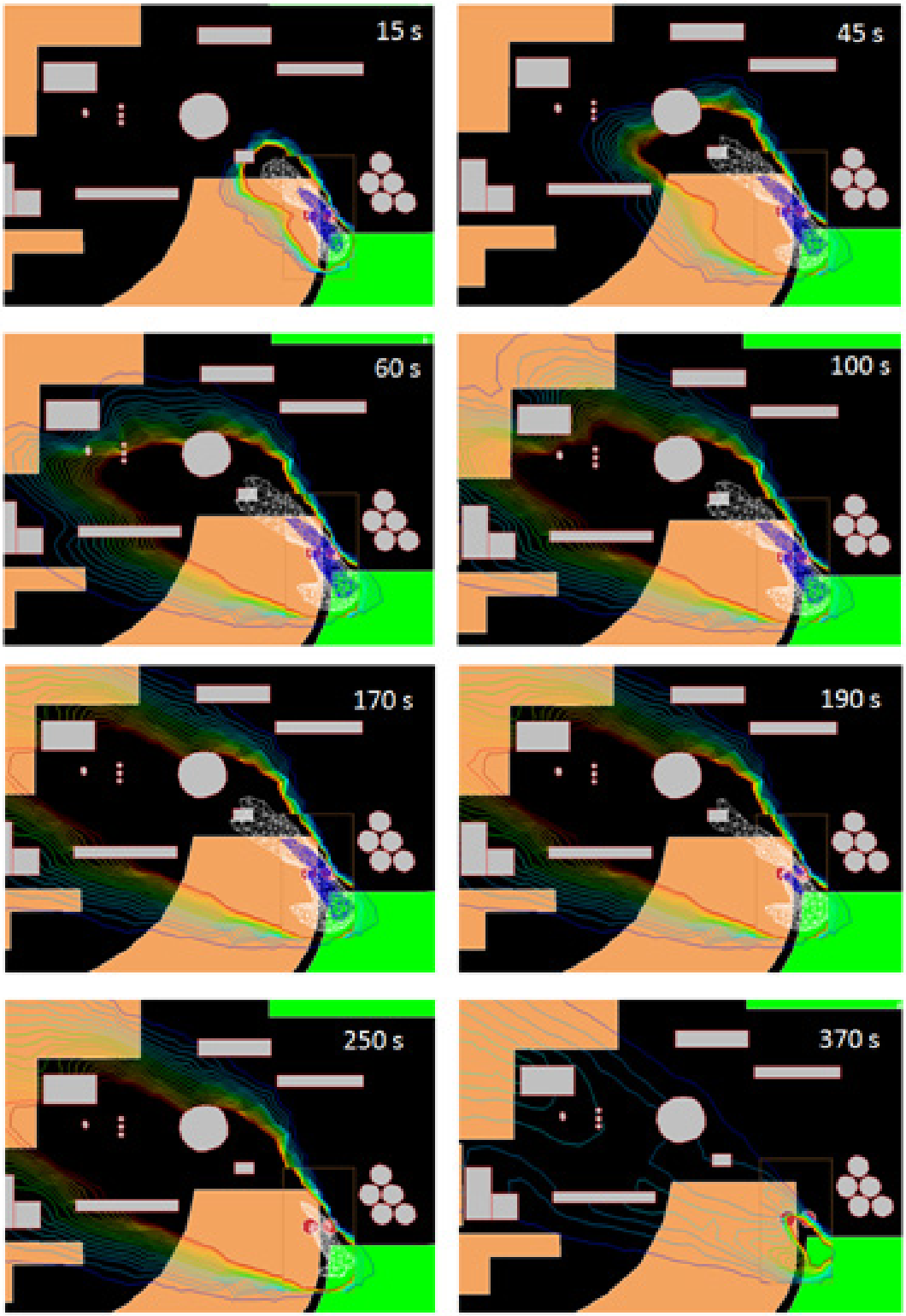

Figure 22. Simulation results showing the CO_2 concentration isopleths (see text) at eight times following the start of the leak for Scenario 3.

Although the source in this double-ended pipe leakage scenario lasts about one third of the time of those in the previous Scenarios, it is interesting to visualize how very high concentrations remain in place for over 5 min. Despite the strong winds, the 10,000 ppm isopleths are in fact much wider relative to the previous Scenarios due to the larger amount of gas released during the first hundred seconds of simulated time.

9.7. Scenario 4

A second scenario of double source-term was modeled in Scenario 4. The release rate modeled was the same as for the previous Scenario 3 (Source B), but the wind velocity considered is much lower. Figures 23 and 24 show the wind field before the release and a result at t = 150 s and sequential shots of the process in 2D, respectively. From Figure 23 it can be seen how the release impinges on the buildings at both sides of the double source. The dispersion of higher concentration is then strongly influenced by the shape and dimensions of the structures. Due to the much lower average wind speed, the gas persist at high concentration for longer than in Scenario 3, but due to the built environment being more open, has a relatively faster dispersion than for Scenario 2 (Source A with dispersion among close buildings).

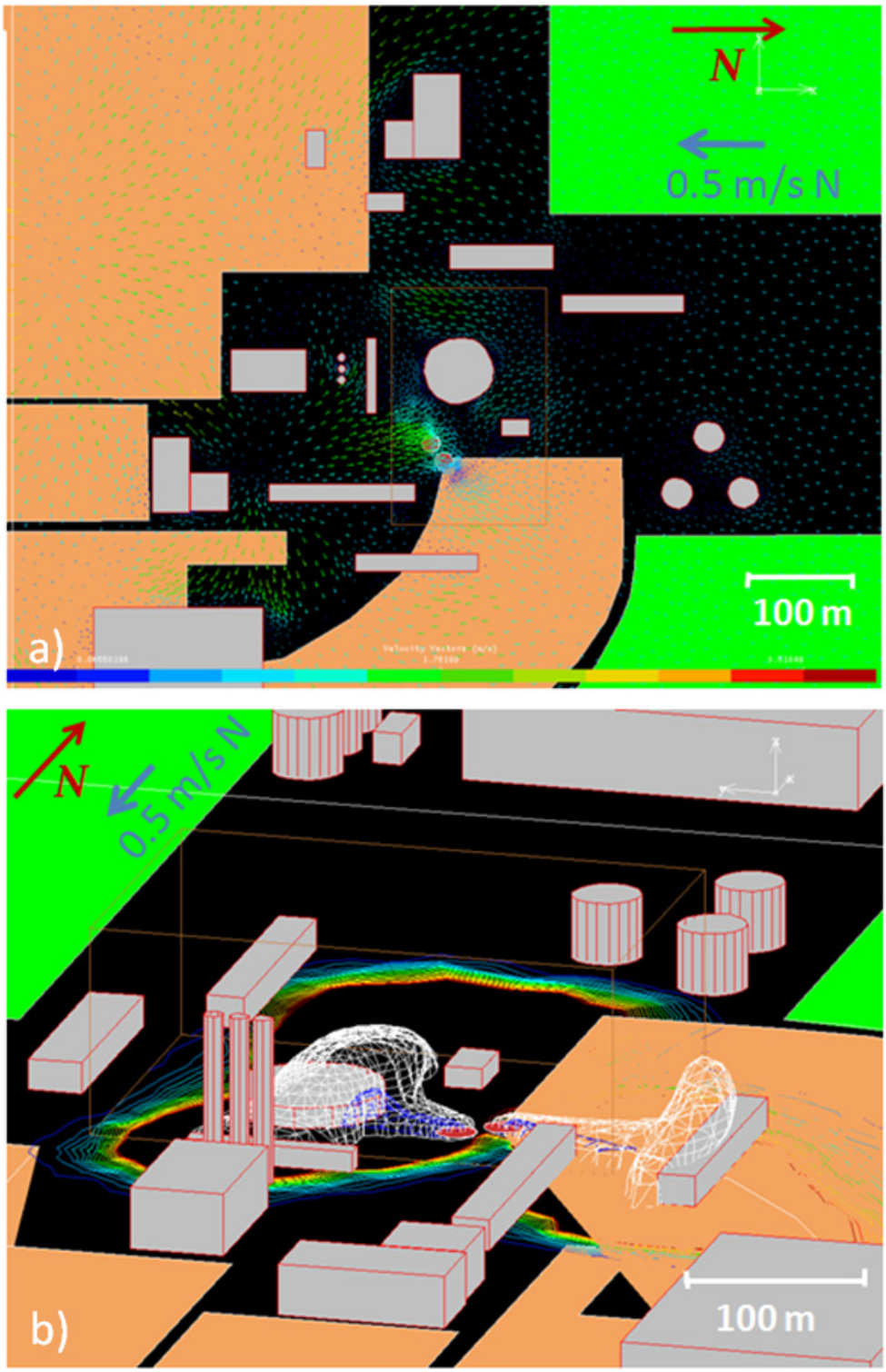

Figure 23. Simulation results for Scenario 4. (a) Wind velocity field in the area of dispersion as modified by the presence of buildings. (b) Oblique view of the model plant showing results at t = 150 s of the 250,000 ppm contour surface (red region near source), the 100,000 ppm contour surface (blue region), 40,000 ppm isosurface (white surface), and 10,000 ppm and lower color contours on the ground surface.

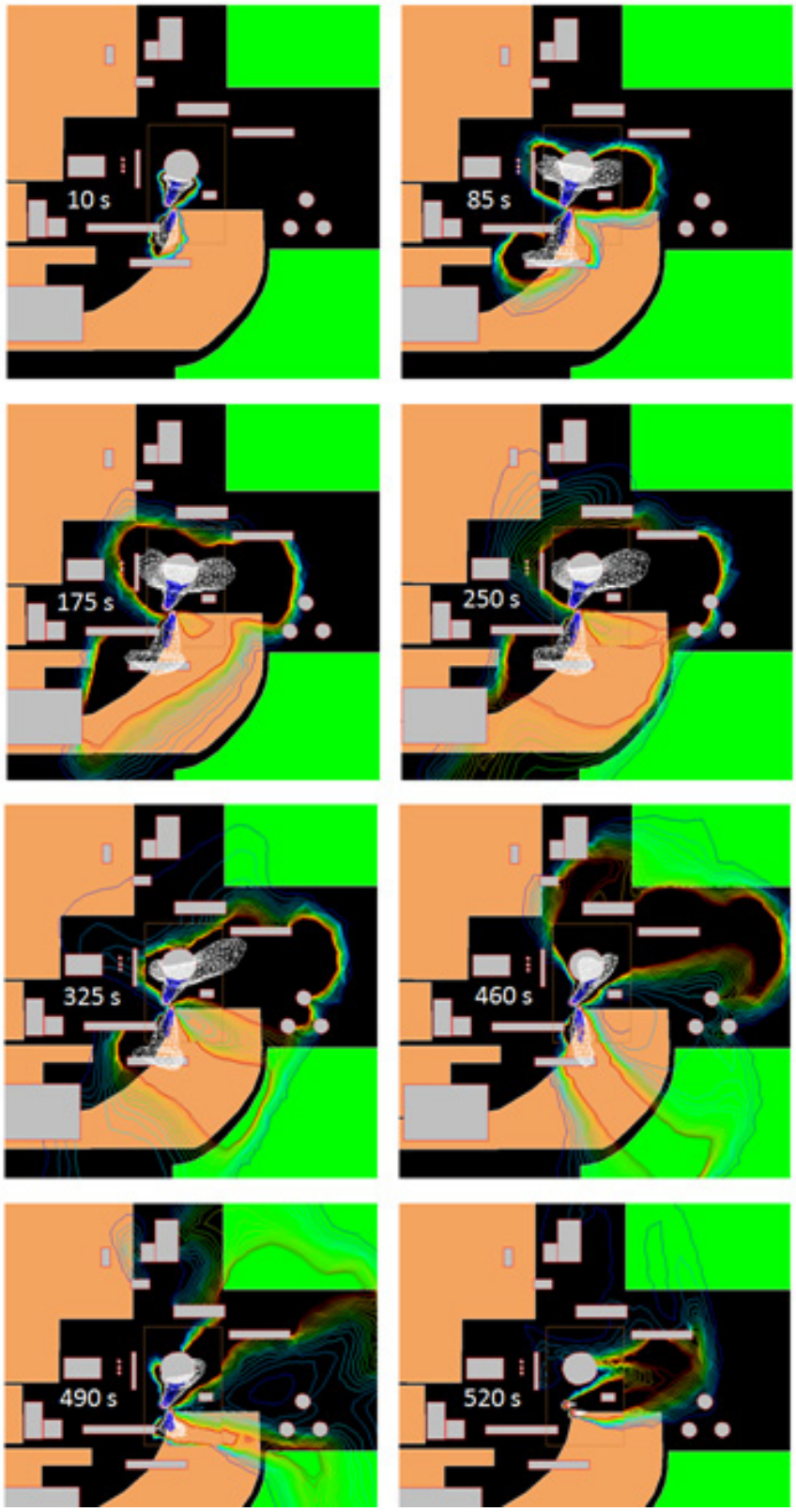

Figure 24. Simulation results showing the CO_2 concentration isopleths (see text) at eight times following the start of the leak for Scenario 4.

9.8. Pressure Blast Exposure Risk

In addition to the hazard presented by CO_2 dispersion, there is also the hazard caused by the shock wave from the blast that occurs at the instant of pipeline failure. In the Energy Institute report (EI, 2010), the authors used the Navier-Stokes equations to evaluate the maximum distance at which the shock wave may be fatal (the fatal pressure change is an informal 700 mbar). We rely on the results of the EI report (EI, 2010) for evaluating this distance. Table 4 gives the data of pipeline diameters for the cases studied by EI (different pipe sizes) and maximum distances covered by the fatal blast. The duration of the blast is on the order of hundredths of a second, i.e., nearly instantaneous after full-bore rupture.

Table 4. Effects of characteristic pressure pulses on humans. Also, the maximum distance of fatal pressure blasts for pipes studied in the EI report are shown (689 mbar = 0.0689 MPa).

mbar	psi	Assumed effect criteria
68,9	1,0	0 % fatality assumed
689	10,0	100 % fatality assumed
Pipe diameter	**Distance reached by fatal blast (689 mbar)**	
8"	5 m	
16"	10 m	
28"	17 m	

From Table 4, considering the dimensions and characteristics of the ADM pipeline (6" diameter), 5 m can be assumed as the distance at which the shock wave from the blast is fatal. This blast is not modeled in our work, but is mentioned here for completeness. The point sources modeled by the CFD code as the CO_2 source term are shown as red dots in Figures 17-22, with a diameter of about 10 m. These circular red regions are therefore approximately the areas of particular danger

due to instantaneous expansion of the shock front (not modeled) in the case of full-bore disruption of the pipe. As explained in the introductory paragraph, the pressure blast could be source of flying debris, extending the hazard to larger distances than the fatal shock.

10. Discussion

In order to have a better understanding of the CO_2 pipeline transportation risk, simulations of CO_2 pipeline leakage scenarios were performed with pipeline leakage rates and velocity of jet flows at the source of the leak calculated with Picard's Pipe model and atmospheric dispersion modeled using a sophisticated CFD model that accounts for density effects. Leakage of the high-pressure CO_2-transporting pipeline recently installed at the ADM ethanol plant was modeled with account taken of the built environment characteristic of this industrial site. The CFD code used for modelling time-dependent dispersion of CO_2, Fluidyn-PANACHE, used distinct terrain scenarios and atmospheric conditions in order to account for the different potential interplays among factors like position of the source term among buildings, turbulence generation and dissipation, and wind speed and direction. To be conservative in the assessment of risks, following the Precautionary Principle, the leaks modeled only comprised full-bore failures (complete breakage of the pipeline along its section), occurring at different distances (locations) from the two ends of the pipeline.

Our approach is novel due to the use of the state-of-the-art Pipe model for the precise quantification of the release rate through time. Prior risk assessments of pipeline leakage hazard have relied on empirically-based or constant release rates approximations (Cameron-Cole, 2005; Kruse and Tekiela, 1996; Turner et al., 2003; Vendrig et al., 2003). Using Picard's isentropic decompression Pipe model in order to have more accurate transient leaking rates, coupled with the use of a sophisticated CFD code for the atmospheric dispersion, makes these simulation results highly defensible. Although the real positioning and direction of a failure are difficult to predict without an exact knowledge of the different human-controlled actions occurring in the plant during normal operations and in accident scenarios, the results presented in this work are

suitable for further study and interpretation, in order to expand their applicability and predictions to other areas of the plant where a leak might be less likely to happen (because of, e.g., lighter vehicular traffic).

A general review of the simulation results reveals how the dispersion of a gas into the ambient air is strongly controlled by the local environmental conditions at the time and place where the release takes place.

The simulations of Scenarios 1 and 2 share the same source term, namely a transient horizontal single source releasing most of the mass during the first hundred seconds but lasting up to 300 s after the leak begins. In view of considering the possibility for the leak to continue without the pipeline being shut off, releases were continued for 200 s more, with a value of 10 m s^{-1} leakage velocity (which is approximately the normal transportation velocity through the system). The first Scenario simulated involved a release in an open area, in which buildings do not present a big issue under the leakage and wind conditions prescribed. The second scenario describes instead a release of the same strength as for Scenario 1 but with leakage occurring within a densely built area. Comparison between the two simulations of the dispersion of the 40,000 ppm and 10,000 ppm isopleths shows the importance of considering the built structures. In the case of medium and high ambient winds, buildings generate turbulence which helps disperse leaking gas. Low wind speed, on the other hand, would make the buildings produce stagnant areas where gas can accummulate at low elevations.

The issue of plume visibility should be considered. It must be noted how the minimum concentration for the plume to be visible is usually set to about 100,000 ppm (10% CO_2 vol, due to the condensation of water vapor (see Figure 4) caused by the very low temperature of the gas

in the plume). Furthermore, the strong noise that a high-pressure full-bore leak would emit, along with the toxic plume being visible, would make bystanders in the area seek help and initiate emergency procedures. Scenario 2 considered the development of the plume above a main road within the plant and towards a location that may present a busy indoor/outdoor working environment. Although, due to the limited amount of CO_2 available for dispersion after a full-bore rupture, the direct influence of buildings on the development of toxic dense gas clouds (100,000 ppm and above) could not be studied in this simulation. However, as mentioned above, the gas could enter buildings and accumulate indoors.

Scenarios 3 and 4 both used a double source term with opposite directions that provide the opportunity to directly compare against single-source release scenarios. The principal differences on the final shapes of the various concentration isopleths analyzed can be highlighted by comparing scenarios with comparable wind speed and different release rates (sources A & B). Plumes generated by Source A are narrower (independent of the direction of the wind) than Source B for which areas affected by hazardous levels of CO_2 are relatively smaller, although in the case of other environmental parameters being identical, the high concentrations last longer. In a direct comparison between cases with Source B, it must be noted that the plumes resulting from the runs are very different: the relatively strong wind simulated for Scenario 3 gives rise to a singular plume with a specific direction, parallel to the wind, that has very little in common with the double plume created under the very low wind of Scenario 4.

The relatively small amount of CO_2 contained in the whole length of the pipeline is the reason that very high gas concentrations (e.g., 250,000 ppm) develop only very near the Source A for a short time. The lethal concentration of 100,000 ppm is, on the other hand, present in each of these simulations and for Source A runs. Its toxicity though is active only after 15 minutes of

continuous inhalation, and it would not prevent workers who find themselves inside the cloud to simply move (walk, run, or drive) out of it, if they are in condition to do so.

A different situation would be faced by people who, at the instant of failure, are standing relatively near to very near the rupture point (say, less than 10 m). Although the concentration of 250,000 ppm does not have a large extent, the high velocity of the flow could knock down a person or expose them to the danger of flying objects, including dry ice chunks, that become airborne in the jet flow. In addition, our simulations show that the plume of 200,000 ppm (which were not displayed in the figures) can reach up to about 50 meters away from the source during the first tens of seconds of release. For some individuals, this cocentration could be fatal in just one minute, while concentrations of 250,000 ppm are fatal to the average person.

We did not model the travel distance that the shock wave created by the fast expanding gas during pipeline rupture. According to EI (2010) this value is 5 meters, a distance that may be alarming when considering that the pipeline passses through relatively busy locations within the plant. As we did not model or investigate any of these shock-wave or pipe-failure processes or mechanisms, we cannot make any definitive conclusions about these processes or risks.

11. Recommendations

The installation of protective guard rails and sturdy posts near the high-pressure pipeline is recommended along roads and in any place the pipe might be particularly vulnerable or exposed to being hit accidentally by vehicles. In the industrial environment considered, road traffic is regulated by strict codes and speed limits which are usually respected. Furthermore, a steel-pipe with 1.5-cm wall thickness would tend to resist damage from car accidents. Nevertheless,

considering the high-risk involved, any measure that could minimize the possibility of the pipe being hit by a vehicle should be considered.

Results of the simulations carried out for this study should be the basis for a careful review of signage, in order to promote constant awareness about the presence of the newly installed high pressure pipeline in workers and visitors. The use of wind socks and other indicators of ambient wind at sites of potential pipeline leakage points would allow workers to quickly identify, during a pipe failure event, upwind and downwind directions in order to minimize exposure to the escaping CO_2.

Capture plants of this kind are likely to be more and more widespread throughout the industrial world in the coming years. Emergency preparedness, response and evacuation procedures, at the ADM site as in other potential capture sites, should be reviewed and possibly standardized for capture and compression operations in addition to transport and final underground injection.

While we have focused here on pipeline CO_2 leakage, there is also a possibility of a well blowout leading to a CO_2 release from the injection or monitoring wells themselves. Such releases would have things in common with the pipeline leak studied here, but would differ in other ways, e.g., by the source being relatively constant for an extended period (depending on how much CO_2 is stored in the reservoir). Therefore, we recommend carrying out a coupled wellbore-reservoir simulations analogous to those of Oldenburg et al. (2011) to calculate possible blowout leakage rates to assess CO_2 plume dispersion for blowout scenarios.

It would be interesting to investigate whether a small high-pressure pipeline rupture would evolve rapidly into a complete rupture of the pipe capable of causing a full-bore rupture, and whether this mode of rupturing (e.g., along welds or weaknesses caused by corrosion) could lead

to the formation of a shock wave. It is also possible that a puncture through the pipe wall could cause the propagation of fractures along the length of the pipe leading to the development of a CO_2 release from a long linear source.

12. Conclusions

A qualitative risk assessment for the ADM transportation system within the Illinois Basin Decatur Project during its working three-year life time was carried out using quantitative and deterministic models of the leakage rate and atmospheric dispersion for representative CO_2 pipeline leakage scenarios. Quantifying the risk for persons due to potential loss of containment of CO_2, e.g. on an annual basis, was not possible. To do this, we would need a model or direct knowledge of the average failure frequency of the system under interest and the values of daily occupancy of the sites where leaks could occur. Both these values are not easely definable and, while the former could experience great variations in time and space, within an average working day, an estimation of the latter can only be derived from past experience, i.e. databases of industrial accidents and considering the vicinity of roads. We used a generic value for failure frequency from the DNV database on pipeline ruptures, namely a probability of 4.65% that, during the three-year lifetime of the IBDP-ADM sequestration project, a full-bore leak could be experienced within the area through which the pipeline runs.

Results show how, overall, the source term ensures that the CO_2 plume concentrations remain low at distances larger than many tens of meters from the leakage site at the ADM plant, even in conditions where the pipe is ruptured across its full diamater (so-called full-bore ruptures) and with low ambient wind. It must be noted however, that if the gas has the chance to intrude into a building at high concentrations, it could accumulate within the indoor environment posing a much larger hazard for people present. On the other hand, the loud noise made by the leak would provide a signal to people inside buidings in the neighbourhood of the pipeline failure to leave the area or take measures to ensure safety, and follow directions from emergency personnel.

As discussed at different points in the text, the risk for a worker of being hit by the shock wave front created after the rupture is dependent on the relative position between the leak and the worker at $t = 0$; persons within a few meters of a catastrophic pipeline rupture may be exposed to a fatal shock wave.

13. References

Amorino, C., Bencini, R., Cara, R., Cinti, D., Deriu, G., Fandino, V., Giannelli, A., Mazzotti, M., Ottiger, S., Pizzino, L., Pini, R., Quattrocchi, F., Sardu, R.G., Storti, G. and Voltattorni, N., 2005, CO_2 geological storage by ECBM techniques; the Sulcis area, Second International Conference on Clean Coal Technologies for our Future Castiadas (Cagliari), Sardinia, Italy.

Atkins, P.W., 2010, Physical Chemistry, 9th ed.: Oxford University Press, ISBN 0199543373.

Barad, M.L., 1958, Project Prairie Grass, a field program in diffusion: Geophysical Research, v. I and II, Air Force Cambridge Research Centre, AFCRC-TR-58-235.

Barrie, J., Brown, K., Hatcher, P.R. and Schellhase, J.J., 2004, Carbon dioxide pipelines: a preliminary review of design and risks, in Fluor, ed.: Calgary.

Burgherr, P. and Hirschberg, S., 2005, Comparative assessment of natural gas accident risks: Switzerland, Paul Scherrer Institut, http://www.dgc.dk/nyhedsservice/pdf/accident_risks.pdf.

Cameron-Cole, 2005, Air dispersion modeling of well blowout and pipeline rupture scenarios. Salt Creek Field, Boulder, Colorado: Prepared for: Howell Petroleum Corporation, Air Dispersion Report JR9/22/2005.

CAPP, 2002, Recommended practice for mitigation of internal corrosion; sweet gas gathering systems: Calgary, Canadian Association of Petroleum Producers.

Chang, J.C. and Hanna, S.R., 2004, Air quality model performance evaluation: Meteorology and Atmospheric Physics, v. 87, 167-196. DOI: 10.1007/s00703-003-0070-7.

Chaudhry, M.H., 1979, Applied hydraulic transients: New York, ISBN 0442215177, 503.

Doss, H.J., Person, H.L. and McLeod, W., 1993, Beware of manure pit hazards, http://nasdonline.org/document/1298/d001097/beware-of-manure-pit-hazards.html, Volume Online library, Michigan State University.

EI, 2010, Technical guidance on hazard analysis for onshore carbon capture installations and onshore pipelines: London, Energy Institute, ISBN 978 0 85293 541 5.

Engebo, A., Nilsen, S., Kirchsteiger, C., Perrette, L., Merad, M. and Andersen, H.B., 2007, Bienal report on hydrogen safety, in Hydro, J., ed.: Risoe, Det Norske Veritas, http://www.hysafe.org/download/1199/BRHS_Chap4_V1p2.pdf.

Folga, S.M., 2007, Natural Gas Pipeline Technology Overview. Decision and Information Science Division. http://corridoreis.anl.gov/documents/docs/technical/APT_61034_EVS_TM_08_5.pdf Argonne National Laboratory. ANL/EVS/TM/08-5

Gale, J. and Davison, J., 2004, Transmission of CO_2--safety and economic considerations: Energy, v. 29, 1319-1328.

Gifford, F.A., 1961, Use of routine meteorological observation for estimating atmospheric dispersion: Nucl. Saf., v. 2, 47-51.

Hanna, S.R., Chang, J.C. and Strimaitis, D.G., 1993, Hazardous gas model evaluation and field observation: Atmos. Environ., v. 27, 2265-2285. ISSN: 1352-2310.

Hirschberg, S., Burgherr, P., Spiekerman, G. and Dones, R., 2004, Sever accidents in the energy sector: comparative perspective: J. Hazardous Materials, v. 111, 57-65.

IEA, 2009, Safety in carbon dioxide capture, transport and storage. IEA, Greenhouse gas R&D programme: Buxton, UK, UK Health and Safety Laboratory. http://co2storage.org/Reports/2009-6.pdf, 128. Report number: 2009/6. .

Jo, Y.-D., and Ahn, B.J., 2002, Analysis of hazard areas associated with high-pressure natural-gas pipelines: J. Loss Prevention in the Process Industries, v. 15, 179-188, PII: S0950-4230(02)00007-4.

Kleine, H., Dewey, J.M., Ohashi, K., Mizukaki, T. and Takayama, K., 2003, Studies of the TNT equivalence of silver azide charges: Shock waves journal, v. 3, 123 - 138.

Koorneef, J., Spruijt, M., Molag, M., Ramirez, A., Faaij, A. and Turkenburg, W., 2008, Uncertainties in risk assessments of CO_2 pipelines, in Elsevier, ed., 9th International Conference on Greenhouse Gas Control Technologies: Washington D.C., USA.

Kruse, H. and Tekiela, M., 1996, Calculating the consequences of a CO_2-pipeline rupture: Energy Conversion, v. 37, 1013–1018.

Kuipjer, M., 2008, MER Ondergrondse opslag van CO_2 in Barendrecht, in B.V., S.C.S., ed.: Deen Haag, Shell CO_2 Storage B.V., http://wwwstatic.shell.com/static/nld/downloads/co2/mer_rapport_2.pdf.

Kuprewicz, R., 2007, Observation on practical: Leak detection for transmission pipelines - an experience perspective, Pipeline Safety Trust: Alaska state, Accufacts Inc, http://pstrust.org/library/docs/leak_detection_paper.pdf.

Mazzoldi, A., 2009, Leakage and atmospheric dispersion of CO_2 associated with carbon capture & storage projects: Nottingham, UK, University of Nottingham.

Mazzoldi, A., Hill, T. and Colls, J., 2007, CO_2 transportation for carbon capture and storage: sublimation of carbon dioxide from a dry ice bank: Int. J. Greenhouse gas Control, v. 2, 210-218.

Mazzoldi, A. and Oldenburg, C.M., 2011, Leakage risk assessment of pipeline transportation of CO_2 at the Illinois Basin Decatur Project, Decatur Illinois, 1st Quarter FY2011 Milestone: Preliminary report on pipeline CO_2 leakage risk assessment, unpublished FY2011 Milestone Report.

Mazzoldi, A., Hill, T. and Colls, J.J., 2011, Assessing the risk of CO_2 transportation within CCS projects, CFD modeling, International Journal of Greenhouse Gas Control, v. 5(4) 816-825.

Mazzoldi, A., Hill, T., and Colls, J.J., 2008, CFD and Gaussian atmospheric dispersion models: a comparison for leakages within carbon dioxide transportation and storage facilities: Int. J. Atmospheric Environment, v. 42, 222-235, DOI: 10.1016/j.atmosenv.2008.06.038.

National Institute of Occupational Safety and Health (NIOSH), http://www.cdc.gov/niosh/idlh/124389.html, accessed February 7, 2013.

Oldenburg, C.M., Freifeld, B.M., Pruess, K., Pan, L, Finsterle, S., and Moridis, G.J., 2011, Numerical simulations of the Macondo well blowout reveal strong control of oil flow by reservoir permeability and exsolution of gas, Proc. National Acad. Sci., Early Edition, July 5, 2011.

Oldenburg, C.M., 2007, Migration mechanisms and potential impacts of CO_2 leakage and seepage, in Gerard, W.A., ed., Carbon Capture and Sequestration Integrating Technology, Monitoring and Regulation, Blackwell Publishing, 127-146, LBNL-58872.

Oldenburg, C.M. and Unger, A.J.A., 2004, Coupled vadose zone and atmospheric surface-layer transport of CO_2 from geologic carbon sequestration sites: Vadose Zone J., v. 3, 848-857, LBNL-55510.

Parfomak, P.W. and Folger, P., 2008, Carbon Dioxide (CO_2) Pipelines for Carbon Sequestration: Emerging Policy Issues, in Service, C.R., ed., CRS Report for Congress, Order Code RL33971.

Pasquetto, S. and Patrone, L., 1994, Comportamento della materia allo stato gassoso: Milano, ISeries S.p.A.

Pasquill, F., 1961, The estimation of the dispersion of windborne material: Met. Mag., v. 90, 33-49.

Pasquill, F., 1974, Atmospheric Diffusion, Ellis Horwood Limited, England

Peng, D.Y. and Robinson, D.B., 1976, A new two-constant equation of state: industrial and engineering chemistry: Fundamentals, v. 15, 59–64, doi:10.1021/i160057a011.

Perry, H.J., 1997, Perry's Chemical Engineer Handbook, McGraw-Hill, 2640.

Perry, R.H., Green, D.W. and Maloney, J.O., 1984, Perry's Chemical Engineers Handbook: London

Picard, D.J. and Bishnoi, P.R., 1988, The importance of real-fluid behavior and nonisentropic effects in modeling decompression characteristics of pipeline fluids for application in ductile fracture propagation analysis: The Canadian Journal of Chemical Engineering, v. 66, 3-12.

Robye, T., Nicholas, H. and Barry, H., 2002, Quantifying the risks associated with a CO_2 sequestration pipeline: Australia.

Rogers, G.F.C. and Mayhew, Y.R., 1980, Engineering thermodynamics work and heat transfer: Essex, UK, Logman Group Ltd.

Schardin, H., 1954, Measurement of spherical shock waves: Communications on pure and applied Mathematics, v. VII, 223-243.

Seiersten, M., 2001, Material selection for separation, transportation and disposal of CO_2, Proceedings Corrosion 2001, Volume paper 01042, National Association of Corrosion Engineers.

Sklavounos, S. and Rigas, F., 2004, Validation of turbulence models for heavy gas dispersion over obstacles: Hazardous Materials, v. A108, 9-20, doi:10.1016/j.jhazmat.2004.01.005.

Stoner, R.G. and Bleakney, W., 1948, The Attenuation of Spherical Shock Wave in Air: Applied Physics, v. 19.

TNO, 1996, Yellow Book: Methods for the calculation of physical effects due to the releases of hazardous material (liquids and gases). in C.J.H. & Wetering, R.A.P.M., ed.: The Haguet, TNO, CPR 14E.

Townes, M.S., Boardman, J.H. and Skinner, R.E., 2004, Pipeline and land use - a risk informed approach: Washington D.C., Transportation Research Board, the National Academies, http://onlinepubs.trb.org/Onlinepubs/sr/sr281.pdf.

Transoft-Int., 2010, PANACHE User Manual: Paris, Saint-Denis

Turner, R., Hardy, N. and Hooper, B., 2003, Quantifying the risks associated with a CO_2 sequestration pipeline: a methodology and case study. Cooperative Research Centre for Greenhouse Gas Technologies (CO2CRC): Camberra.

USA, 2004, Code of Federal Regulations, Government, United States of America.

Vendrig, M., Spouge, J., Bird, A., Daycock, J. and Johnsen, O., 2003, Risk analysis of the geological sequestration of carbon dioxide, in Crown, ed., Volume R246 DTI/Pub URN 03/1320 Department of Trade and Industry's Cleaner Coal Technology Transfer Programme.

Wakes, S.J., Holdo, A.E. and Meares, A.J., 2002, Experimental investigation of the effective orifice shape and fluid pressure has on high aspect ratio cross-sectional jet behaviour: Hazardous Materials, v. 1, PII: S0304-3894(01)00307-7.

Yuhua, D., Huilin, G., Jing'en, Z. and Yaorong, F., 2002, Evaluation of gas release rate through holes in pipelines: J. Loss Prevention in the Process Industries, v. 15, 423-428, PII: S0950-4230(02)00041-4.

Zhang, Z.X., Wang, G.X., Massarotto, P. and Rudolph, V., 2006, Optimization of pipeline transport for CO_2 sequestration: Energy Conversion and Management, v. 47, 702-715, doi:10.1016/j.enconman.2005.06.001.

Appendix A. Experience with Pipeline Transportation of CO_2

In the last 35 years, CO_2 has been used by the oil industry for enhancing the production of hydrocarbons via the restoration of the pressure gradient and enhancing mobility of oil in depleting oil and gas reservoirs (Amorino et al., 2005). A significant CO_2 transportation infrastructure has developed to meet this need. Altogether, 6,000 km of CO_2 pipelines are being operated in the USA primarily for Enhanced Oil Recovery (EOR), transporting a total of more than 80 Mt y^{-1} of CO_2 (Koorneef et al., 2008). To make a comparison, in the USA there are over 2 Mkm of natural gas transportation pipelines and more than 250,000 km of hazardous liquid pipelines (anhydrous ammonia, crude oil, fuel oil, diesel fuel, condensate, gasoline and others) (Gale and Davison, 2004). The experience gained in moving hazardous liquids can be applied to the transportation of CO_2, taking into account the particular behavior of this fluid when a leakage from a superficial/shallow facility occurs.

CO_2 is a commonly used industrial material. The design implications for transporting CO_2 compared to other gases appear to be well understood (Barrie et al., 2004; Gale and Davison, 2004; Zhang et al., 2006). CO_2 pipeline operators have designed minimum specifications for flow composition. The mechanical requirements for CO_2 pipeline design are subject to standards, the major one being the USA Code of Federal Regulations, Parts 190-195 (USA, 2004). The design, material, and construction issues related to the safe operation of CO_2 pipelines are regulated under the 2001 Code of Federal Regulations, Parts 190–199 (Parfomak and Folger, 2008). A point to note is that under federal regulations in the U.S., CO_2 pipelines are classified as high volatile/low hazard and low risk (due to the product being nonflammable). As a matter of public record, during the period 1991 to 2001, there were no CO_2 pipeline-related injuries or deaths (EI, 2010).

Carbon dioxide is an acid gas and will react with water to form carbonic acid in conditions of low H_2S concentration; carbonic acid corrosion of carbon steel has been recognized for years as a major source of damage in oilfield equipment and gas pipelines, and is commonly referred to as "sour corrosion" (Barrie et al., 2004; CAPP, 2002). Internal pipeline corrosion is an important cause of gas loss in gas transportation: it can pose serious problems in systems transporting pure CO_2.

Dry carbon dioxide does not corrode the carbon-manganese steel generally used for pipelines (the absence of water reacting with carbon dioxide preventing the formation of carbonic acid), due to the CO_2 stream being "dry" – i.e. <0.5 gH_2O $(Nm^3CO_2)^{-1}$ (Rogers and Mayhew, 1980). Seiersten calculated that over a 12-year period, the corrosion rate in an operating dry CO_2 pipeline amounts to 0.25-2.5 μm yr^{-1} (Seiersten, 2001).

Because of the Joule-Thomson effect, CO_2 cools dramatically during decompression potentially allowing CO_2 to change from gaseous or liquid conditions to solid (dry ice), so pressure and temperature must be controlled continuously. To be transported in a pipeline CO_2 must be compressed to ensure that single-phase flow is achieved. The most widely used operating pressure is between 1,090 and 3,090 psi (7.4 and 21 MPa). Above 1,090 psi (7.4 MPa), CO_2 exists as a single dense phase over a wide range of temperatures (i.e., either super-critical if above 88 °F (31 °C) or liquid if below this temperature). Clearly, a transmission pipeline, especially if above ground, can experience a wide range of ambient temperatures, so it can be challenging to minimize density variations. If the pressure becomes lower than 1,090 psi (7.4 MPa), gaseous and liquid conditions (two-phase conditions) could arise in the pipe depending on the temperature with resulting pressure surges and flow blockages (Barrie et al., 2004).

In long pipelines, it is necessary to estimate the pressure drop along the pipeline so that compression stations can be placed at appropriate intervals to prevent the choke point being reached when two-phase flow occurs in the pipeline. The pressure drop is dependent on the temperature, flow rate and geometric characteristics of the pipeline such as diameter, length, and elevation changes (Zhang et al., 2006). Usually, oil industry practice in control methodology is to use an automatic control system to monitor volumetric flow rates and pressure fluctuations in the pipeline, coupled with block valves (ESD) at set distances that can be shut off in the event of pipeline failure (Gale and Davison, 2004; Robye et al., 2002).

A.1. Seismic hazard for pipeline systems

The principal earthquake hazards for pipeline systems include ground failure due to liquefaction or landslides and ground shaking effects on above-ground facilities and equipment. Ground settlement and seismic wave propagation are less important effects, but could possibly affect buried pipelines in certain special circumstances. Surface fault rupture is also potentially hazardous to pipelines, in general, but there is no evidence of active faults in southern Illinois that might affect the planned route of the CO_2 pipeline. The potential effects of the various earthquake hazards on the CO_2 pipeline are estimated in this report, considering simulations of full-bore leaks from the transportation system (as in EI, 2010).

Transmission pipelines are typically buried under a soil cover of 3 to 4 ft (~ 1 m) or deeper in agricultural areas. Burial tends to make a pipeline more susceptible to large permanent ground distortions such as landslide or liquefaction-induced ground displacement. The effects of seismic ground movement along a pipeline route are generally sporadic, depending on local soil, groundwater, and topographic conditions. The nature of the ground displacements are not well

defined and generally can occur at any point within an area of potential movement. The amount of ground displacement depends largely on the intensity and duration of earthquake ground shaking.

Appendix B. Pipe decompression model

The transient leak rate from the studied CO_2 pipeline were predicted using the one-dimensional, non-isentropic, real-fluid blowdown simulation model developed by (Picard and Bishnoi, 1988). This model is based on the basic one dimensional unsteady-state Navier-Stokes continuity, momentum balance and energy balance equations uniquely expressed in terms of the fluid velocity, density and pressure of the following three state variables to facilitate convenient run-on implementation of a real fluid equation of state to predict the thermodynamic properties and phase behavior of the fluid. The developed Navier-Stokes partial differential equations are presented below and comprise the following inherent assumptions: the fluid flow is one-dimensional, frictional forces are only acting on the fluid at inside surface of the pipe wall, there is heat transfer through the pipe wall from the surrounding environment to the fluid and the fluid is always in thermodynamic equilibrium:

<u>Compatibility Equation</u>

$$\frac{D\rho}{Dt} + \rho\frac{\partial u}{\partial x} = 0$$

<u>Momentum Conservation Equation</u>:

$$\rho\frac{Du}{Dt} + \frac{\partial P}{\partial x} = -2C_f\rho\frac{u|u|}{D_p}$$

<u>Energy Conservation Equation</u>:

$$\frac{DP}{Dt} - a^2\frac{D\rho}{Dt} = e\frac{2C_f\rho u^3 + 4U(T_\infty - T)}{D_p\rho T}$$

In the above equations t and x denote time since the start of the leak and axial position in the pipeline, while D_p denotes the pipe diameter and ρ, P, T and a are the local fluid density, pressure, temperature and sound velocity. The term D/Dt is the substantial differential operator

$\frac{\partial}{\partial t} + u\partial/\partial x$. C_f is the Fanning friction factor. T_∞ is the temperature of the material surrounding the pipe. And the variable e denotes the term $\left(\frac{\partial P}{\partial s}\right)_\rho$, where s is entropy.

For improved numerical accuracy, the developed Navier-Stokes partial differential equations were transformed into the ordinary differential equations by using the Method of Characteristics. These characteristic equations were solved using the implicit finite-difference scheme described in (Chaudhry, 1979).

The fanning friction factor for the calculation of the frictional force at the wall was computed using Chen's correlation for transitional and turbulent flow and the relation $f = 16/\mathrm{Re}$ (where Re is the Reynolds number) for laminar flow. Similarly, coefficients for heat transfer between the fluid and the inside pipe wall were calculated using the following correlations (Perry, 1997):

- For laminar flow conditions (i.e., Reynolds number ≤ 2,100) Hausen's correlation was used for Graetz numbers less than 100, and the Sieder-Tate correlation is used for Graetz numbers greater than or equal to 100.
- For transition regime flow conditions (i.e., Reynolds number between 2,100 and 10,000), Hausen's correlation was used.
- For turbulent flow conditions (i.e., Reynolds number ≥ 10,000), the Sieder-Tate correlation was used.

The presence of a valve was modeled as a convergent-divergent section with the valve orifice in the midpoint of the fluid flow path length inside the valve.

Two different real-fluid equations of state are used to estimate the thermodynamic properties and phase behavior of the CO_2: (1) a multi-component Equation of State (EOS) by (Peng and

Robinson, 1976) which allows the presence of some impurities in the CO_2 to be considered (e.g., N_2, H_2S, and CH_4), and (2) the ANSI EOS for pure CO_2. The first EOS is only able to consider gas-liquid phase behavior, while the second EOS is able to consider gas-liquid-solid phase behavior.

Appendix C. Fluidyn PANACHE, model description

Atmospheric dispersion modeling is a subset of computational fluid dynamics that involves the mathematical simulation of how air pollutants disperse in the atmosphere by advection and diffusion under laminar and turbulent flow processes. Here we describe the commercial CFD code by Fluidyn (http://www.fluidyn.com/fluidyn/) called PANACHE/PANEPR.

Fluidyn-PANACHE (version 4.0.7) is a computer code for numerical simulation of atmospheric flows and pollution in short and medium-range scales. PANACHE uses CFD tools (i.e. Navier-Stokes equations and turbulence models) in a finite volume based approach, solving the differential equations governing mass, momentum, and energy transfer on discrete CV's, provided by a non-uniform mesh generator that accounts for the presence of obstacles or topographical features (i.e. with generation of a finer mesh in critical areas).

C.1. Navier-Stokes Equations

The equations solved by PANACHE are the following. First, the continuity equation for total fluid density is given by:

$$\frac{\partial \rho}{\partial t} + \nabla \bullet [\rho u] = \delta_s + \delta_p \qquad \text{(C1)}$$

Where ρ is the density of CO_2 for a gaseous state (kg m^{-3}); u is wind speed (m s^{-1}); ∇ denotes the gradient of the considered quantity on the three dimensions; δ_s and δ_p are source terms for species (CO_2 in this case) due to (s) pollutant emission, (p) droplet evaporation/condensation (kg m^{-3} s^{-1}).

The momentum equation for the fluid mixture is:

$$\frac{\partial \rho u}{\partial t} + \nabla \bullet [\rho u u + \sigma] = \nabla P + F_s + F_g + F_p \qquad \text{(C2)}$$

where σ = Newtonian viscous stress tensor = $\mu[\nabla u+(\nabla u)^T]+\lambda(\nabla \bullet u)i$, where μ and λ = first and second coefficients of viscosity, $\lambda = -2/3\mu$; T = matrix transpose; i = unit dyadic - product of vectors); P is fluid pressure; F_s is the rate of momentum gain per unit volume due to pollutant emissions (N m^{-3}) and F_g and F_p are forces due to: (g) gravitational acceleration, (p) interactions with droplets/particles (N m^{-3})

The internal energy equation is:

$$\frac{\partial \rho I}{\partial t} + \nabla \bullet [\rho u I + J] = \nabla \bullet u + \rho \varepsilon + Q_s + Q_p + Q_h \qquad \text{(C3)}$$

where I is specific internal energy (J Kg^{-1}); J = heat flux vector = $k_c \nabla.T + \rho\Sigma[h_m \nabla(\rho_m/\rho)]$, (W m^{-2}); $Q_s/_p/_h$ are rates of specific internal energy gain due to: (s) pollutant emission, (p) interaction with particles, (h) surface energy budget (J Kg^{-1} s^{-1})

PANACHE solves the governing equations described above both in three-dimensional space and in time. The spatial differentiation is done over a three-dimensional mesh made up of arbitrary hexahedrons. A control-volume or integral-balance approach is used to construct the finite difference approximations for each of these control-volumes to preserve local conservation of differenced quantities. The time differentiation enables a unified approach towards both transient and steady state phenomena and is carried out over a sequence of time steps. An implicit procedure enables the use of unlimited time steps.

C.2. Turbulence models

Two turbulence models (k-ε and k-l models) are used by PANACHE depending on the atmospheric conditions (k-ε for stable and k-l for unstable atmospheric conditions). The standard k-ε model (Sklavounos and Rigas, 2004) is modified to include the effects of buoyancy and the stability of the atmosphere by means of the Richardson number (the non-dimensional parameter characterizing the stability of the atmosphere in terms of temperature), defined as:

$$Ri = \frac{g}{T} * \left(\frac{\partial \theta}{\partial z} \right) * \frac{\rho}{G} \qquad \text{(C4)}$$

Where T is temperature (K); θ is potential temperature (K); z is height and G is turbulence production rate by shear, $G = \sigma \nabla u$ (kg m^{-3} s^{-2}). Ri is negative for unstable conditions and positive for stable conditions.

The equations for k (turbulence generation) and ε (turbulence dissipation) are given below:

$$\frac{\partial \rho k}{\partial t} + \nabla [\rho u\, k - (\frac{\mu}{\sigma_k}) \nabla k] = \frac{2}{3} \rho k \nabla * u + G\, (l\, \frac{Ri}{\sigma_h})\, \rho \varepsilon + W_p \qquad \text{(C5)}$$

where σ_h is the Prandtl number which for the k-ε model = 1.11; μ is the primary (shear) viscosity of the fluid (Kg m^{-1} s^{-1}); $\sigma_{k/\varepsilon}$ are dimensionless turbulence model constant for the k and ε equations, equals to 1.0 and 1.2, respectively; σ_h is the dimensionless turbulent Prandtl number; W_p represent the turbulence production due to interaction with particles (m^2 s^{-3}) and C_1 and C_2 are k-ε turbulence model dimensionless constant equal to 1.44 and 1.92 respectively. The turbulent viscosity is given by:

$$\nu_t = C_E * \frac{k^2}{\varepsilon} \qquad \text{(C6)}$$

The *k-l* model is a one-equation model where Equation (C5) for k is solved while the turbulent length scale is specified algebraically. σ_h in Equation (C5) for the present model is not constant but is a function of Ri. Equation (C6) is not solved and ε in equation (C5) is defined as: $\varepsilon = C_D \cdot k^{3/2}/l$. The length scale, l, is prescribed algebraically for different atmospheric stability conditions: stable (E, F) unstable (A, B) and neutral (C, D). The turbulent viscosity is given as: $\nu_t = C_\mu \cdot k^{1/2}\, l$.

It must be said that, within jet release simulations, no difference is found between the utilization of the two models, concerning the downwind length of highly concentrated plumes.

C.3. Boundary conditions

Boundary conditions are specifications of properties on the surfaces of the domains and are required to fully define the flow simulation. Ambient mean wind speed and air temperature profiles are boundary conditions (supposing they are constant over the domain area), represented by logarithmic functions for all the trials in this study. Such that:

$$v(z) = \frac{u^*}{\kappa}[ln(\frac{z}{z_o})\ \Psi_1(\varsigma)] \qquad \text{(C7)}$$

$$\theta(z) = \sigma_h \frac{\theta^*}{\kappa}[ln(\frac{z}{z_o})\ \Psi_2(\varsigma)] \qquad \text{(C8)}$$

where θ^* = temperature scale; $\Psi_1(\varsigma)$ and $\Psi_2(\varsigma)$ = similarity profile. The surface friction velocity, u^*, the temperature scale θ^*, and the Monin-Obukhov length, L are related by: $L = u^{*2}T / (g\ \kappa\ \theta^*)$ and $\theta^* = Q_h / (\rho\ C_p\ u^*)$; where κ is Von Karman constant = 0.41, T is temperature, σ_h is the turbulent Prandlt number, dimensionless, and Q_h is the sensible heat flux (J Kg^{-1} s^{-1})

The micrometeorological parameters, u^*, θ^*, and L are evaluated for different atmospheric stability classes. For unstable and neutral conditions $u^* = U^* [1+a \ln(1+bQ_0/Q_1)]$, where $U^* = \kappa v/\ln(z_m/z_0)$ is the friction velocity for neutral conditions, $m = 4h_{an} z_0$, h_{an} = anemometer height, $Q_0 = Q_h/(\rho C_p)\ Q_1\ \theta U^{*3}/(\kappa g\ z_m)$, θ = potential temperature, a and b are constants dependent on z_0 and z_m. For stable conditions, Equations (C7) and (C8) are solved in L and the other parameters are found via their relationships.

Ground roughness is another boundary condition which can vary greatly with the nature of the area considered (presence of fields, forests, water bodies, etc.) and the presence of small artifacts (generally, small buildings are not considered individually but only in terms of increased ground roughness). In this study, PANACHE was given a surface roughness length z_0 = 0.5 m within the plant environment. This value is used with the aim of accounting for smaller buildings and well sized obstacles (e.g. general purpose pipelines, working vehicles and general mechanical apparatuses).

C.4. Site data incorporation by PANACHE

Here it is given a brief introduction to how PANACHE accounts for topographical features (ground shape, building and land uses) and meteorological parameters.

C.4.1. Terrain characteristics

Terrain topography strongly affects the wind flow patterns as well as the turbulence characteristics that have a direct bearing on pollutant dispersion. Terrain undulations and buildings in fact determine the wind flow patterns; terrain features such as vegetation and urban canopies affect local turbulence, mixing and thermal/hygroscopic behavior of air; vegetation canopies also result in deposition of pollutants on leaf surfaces, urban canopies release additional

heat due to human activities and also some emissions; water bodies tend to act as heat sinks during daytime and heat sources during night, due to differential heating of the soil and water.

Terrain topological definition in PANACHE can be broadly classified into the following types: site data, altitude curves that define the terrain undulations, buildings and obstacles and land use data. Terrain features can be created on PANACHE tracing them from a map or directly creating them. In this study, a large amount of topographical data and building disposition within the plant has been taken from overhead photos, with length scales parameters given by Google Earth.

The structure of the Planetary Boundary Layer (PBL) depends on the ground roughness and the sensible heat flux released into the atmosphere from the ground. The sensible heat flux depends on the incoming solar radiation, the surface moisture availability factor, surface albedo and surface emissivity: these surface characteristics vary with land use. Types of predominant land use can be set by the user.

PANACHE uses a 3-dimensional curvilinear mesh for the study area on which the Navier-Stokes equations are solved. The base of the 3D mesh exactly matches the terrain undulations defined through altitude curves. A detailed description of mesh generation within the model can be found in PANACHE User Manual (Transoft-Int., 2010).

C.4.2. Meteorological inputs

The planetary boundary layer is the region of the atmosphere near the ground surface where the influence of the surface is felt on a time scale of 1 hour or less through turbulent exchange of momentum, heat and moisture (Transoft-Int., 2010). The equations which describe the large-scale evolution of the atmosphere (equations 10-3 and 10-4 in the user's guide) do not take into

account the interaction with the surface. The turbulent motion responsible for this interaction is small-scale and totally sub-grid and therefore needs to be parameterized (modeled).

The PBL model serves as the interface between the meteorological observations and the boundary conditions required by the CFD solver. It is composed of two parts:

- A micrometeorology model that computes fundamental physical characteristics of the PBL from observations;
- A boundary layer model for prescribing the vertical profiles of wind speed, temperature, and turbulence.

PANACHE needs the meteorological data in the study area. These are:

- Surface observations:
  - Wind speed and direction
  - Temperature
  - Pressure
  - Cloud cover
  - Humidity
- Vertical structure of the PBL:
  - Profile of wind speed
  - Profile of temperature

The above meteorological data can be constant for the duration of simulation or varying with time. The constant data are fed in the menu itself. Atmospheric stability conditions are not directly fed by the user but are dependent on the time of the day in which the simulation is taking place and the cloud cover (due to the heat from the ground).

C.5. PANACHE. Validation and verification

The atmospheric dispersion model PANACHE (Version 3.4.1) has been evaluated against the dispersion field experiments Prairie Grass and Kit Fox (Mazzoldi et al., 2008), following the directives for atmospheric dispersion model performance measures suggested by Hanna et al. (1993) and summarized by Chang and Hanna (2004). PANACHE was used to simulate releases of a buoyant tracer gas (SO_2) on flat terrain (that is, the Prairie Grass field experiments) and releases of a dense gas (CO_2) on terrain with obstacles (the Kit Fox field trials), in order to simulate an industrial plant scenario. Both field experiments consisted in the release of certain amounts of pollutant and the measurement of maximum downwind gas concentrations by samplers installed at different distance from the source (Figure C1). With the aim of considering the highest downwind concentration, in order to account for the variability of wind direction, samplers were installed at different heights along concentric arcs at set distances: the concentration data used were the highest recorded ones.

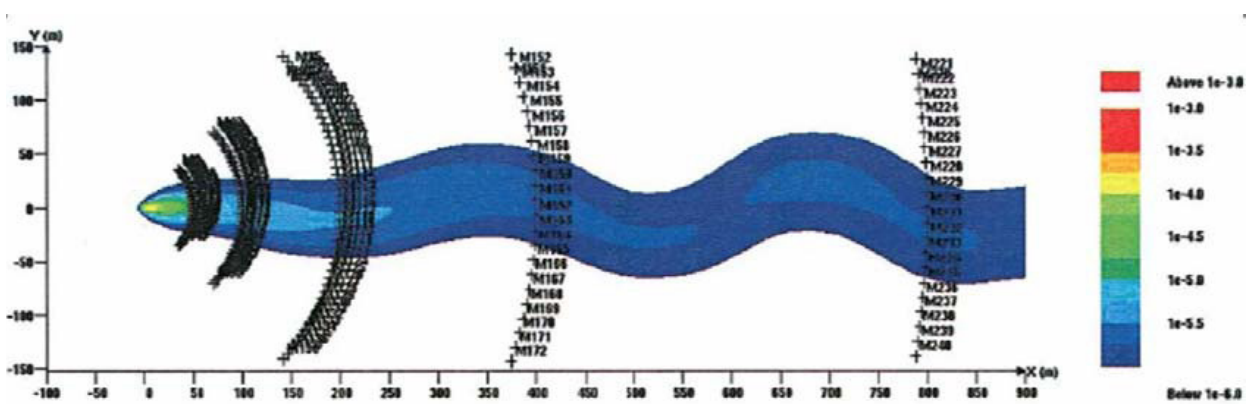

Figure C1. Locations of five arcs (x = 50, 100, 200, 400, and 800 m) in the Prairie Grass experiment (Barad, 1958).

The code PANACHE gave very good results over about 100 trials composing the validation exercise (Mazzoldi et al. 2008), making it a good choice for CO_2 dispersion modeling in

hazardous locations. The code has been recently used for modeling jet releases from high-pressure pipeline transporting CO_2 (Mazzoldi, 2009; Mazzoldi et al. 2011).

DISCLAIMER

This document was prepared as an account of work sponsored by the United States Government. While this document is believed to contain correct information, neither the United States Government nor any agency thereof, nor The Regents of the University of California, nor any of their employees, makes any warranty, express or implied, or assumes any legal responsibility for the accuracy, completeness, or usefulness of any information, apparatus, product, or process disclosed, or represents that its use would not infringe privately owned rights. Reference herein to any specific commercial product, process, or service by its trade name, trademark, manufacturer, or otherwise, does not necessarily constitute or imply its endorsement, recommendation, or favoring by the United States Government or any agency thereof, or The Regents of the University of California. The views and opinions of authors expressed herein do not necessarily state or reflect those of the United States Government or any agency thereof or The Regents of the University of California.

Ernest Orlando Lawrence Berkeley National Laboratory is an equal opportunity employer.